Fatigue behavior evaluation of full-scale OSD-UHPC composite bridge deck system

Shi, Zhanchong; Su, Qingtian; Kavoura, Florentia; Veljkovic, Milan

DOI
10.1016/j.engstruct.2022.115179

Publication date
2023

Document Version
Final published version

Published in
Engineering Structures

Engineering Structures 275 (2023) 115179

Contents lists available at ScienceDirect

Engineering Structures

journal homepage: www.elsevier.com/locate/engstruct

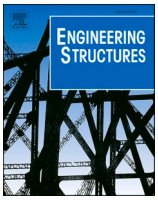

Fatigue behavior evaluation of full-scale OSD-UHPC composite bridge deck system

Zhanchong Shi [a,b], Qingtian Su [a,c,*], Florentia Kavoura [b], Milan Veljkovic [b]

[a] Department of Bridge Engineering, Tongji University, Shanghai 200092, China
[b] Department of Engineering Structures, Delft University of Technology, 2628CN Delft, The Netherlands
[c] Shanghai Engineering Research Center of High Performance Composite Bridges, Shanghai 200092, China

ARTICLE INFO

Keywords:
OSD-UHPC composite deck
Fatigue damage
S-N curve
Fatigue behavior evaluation
Fatigue strength

ABSTRACT

To investigate the fatigue performance and fatigue damage process of the Orthotropic Steel Deck (OSD) - Ultra-High Performance Concrete (UHPC) composite bridge deck, a two-span continuous full-scale specimen was designed and tested under cyclic loading. Test results showed that the fatigue cracks firstly initiated near the lower part of the weld toe of the rib-to-cross beam welded joint, and then cracks along the weld length of the U-rib butt-welded joint developed. These observations followed by the OSD-UHPC interface debonding. The U-rib bolted joint exhibited better fatigue resistance than the U-rib butt-welded joint. The *S-N* curves of the rib-to-cross beam welded joint, the U-rib butt-welded joint and the U-rib bolted joint were established based on existing fatigue test data, and were compared with provisions in design codes. The *S-N* curves from the beam test for the short-headed stud connectors were compared with that from the push-out test. And the established *S-N* curves with 95% survival probability from the push-out test could be used to assess the global fatigue performance of the composite deck. Considering the durability-based critical crack width of UHPC, the established tensile *S-N* curve regarding critical UHPC crack width of 0.05 mm could be used to evaluate the anti-fatigue cracking ability of the UHPC layer in the composite deck system.

1. Introduction

Orthotropic steel bridge decks (OSDs) have been widely used in long-span bridges owing to the low self-weight, the high load-carrying capacity and the easy installation [1]. The OSD consists of the steel deck plate, the longitudinal U-shaped ribs (parallel to traffic flow), and the transverse cross beams (perpendicular to traffic flow), which are connected together by welding. The OSD is usually covered with a thin layer of asphalt pavement. Under the ever-increasing traffic volumes and higher vehicle wheel loads, serious fatigue cracks occur at fatigue-prone details in OSD, such as the rib-to-deck plate welded joint, the rib-to-cross beam joint, the rib longitudinal splice joint and the cross beam cutout [2]. The main reasons for these fatigue cracks are [3–6]: (1) insufficient local stiffness of the deck, (2) welding initial defects and residual stress, and (3) serious stress concentration induced by inappropriate geometric details.

To solve or alleviate the fatigue cracking problems of the OSD, steel–concrete composite bridge deck [3,7], has been proposed by adding the rebar reinforced concrete layer to the OSD. The enhanced local stiffness of the OSD is achieved through the composite effect provided by the OSD-concrete interface connections, such as the epoxy adhesion [7,8], the combination of epoxy adhesion and sparsely distributed welded studs [9], and the densely distributed welded studs [3,10]. In real practice, ultra-high performance concrete (UHPC) is preferred as the concrete material in the composite deck considering the mechanical properties as well as the durability. UHPC is designed based on the dense particle packing theory, and is characterized by a water-to-binder ratio less than 0.25, compressive strength greater than 120 MPa or 150 MPa, sustained post-cracking tensile strength greater than 5 MPa, modulus of elasticity greater than 45 GPa and excellent durability [11–13]. Owing to the robust composite action achieved by the densely distributed welded studs and the exceptional mechanical properties and durability of UHPC, the OSD-UHPC composite bridge deck is becoming increasingly popular in the retrofitting of old-cracked steel bridges and the design of new steel bridges over the last decade in China [14–18].

Full-scale tests have been conducted to investigate the static and fatigue behavior of the OSD-UHPC composite deck. Dieng et al. [10] performed comparative tests of the OSD and the OSD-UHPC composite

* Corresponding author at: 1239 Siping Road, Tongji University, Shanghai 200092, China.
E-mail address: sqt@tongji.edu.cn (Q. Su).

https://doi.org/10.1016/j.engstruct.2022.115179

Available online 17 November 2022

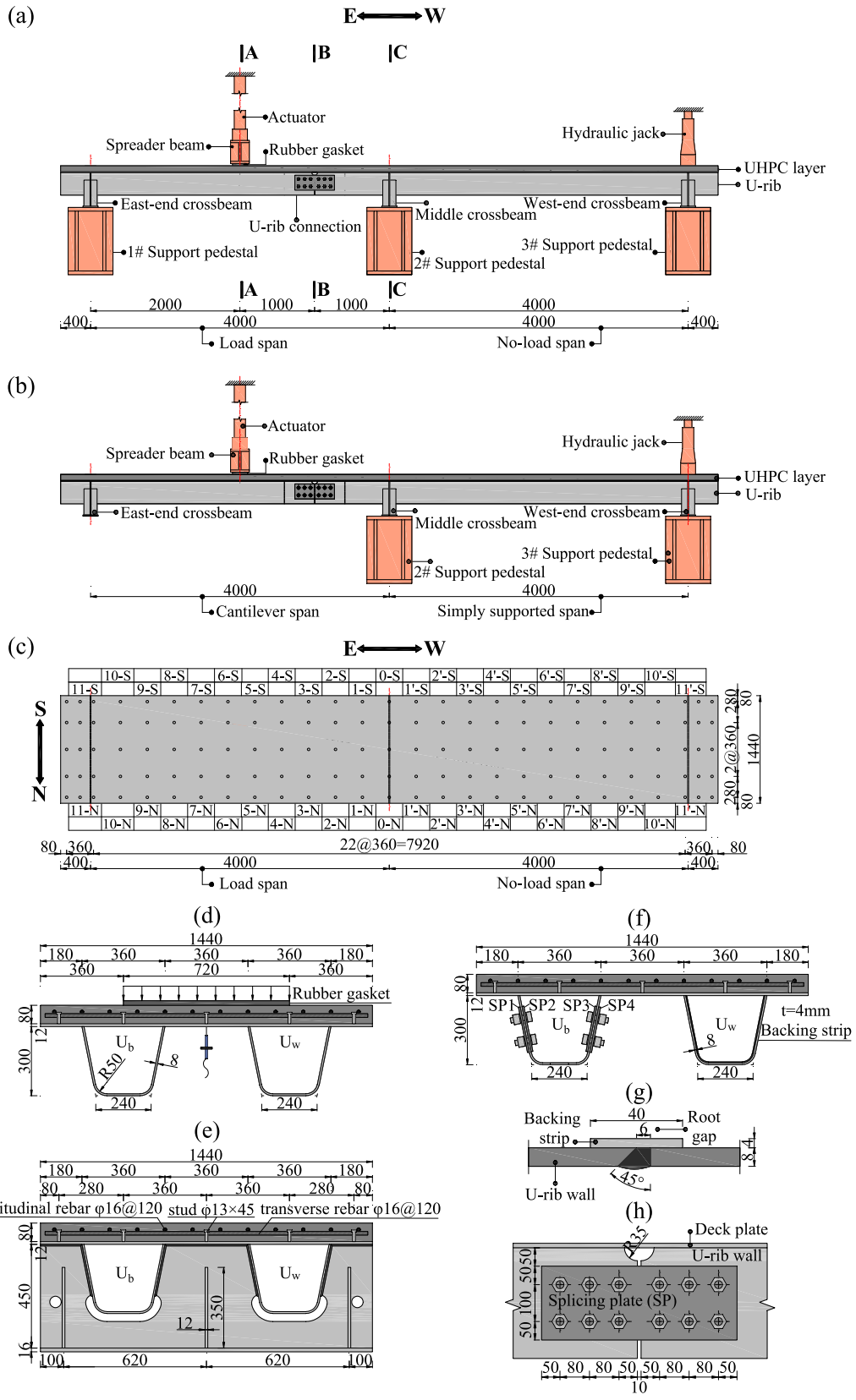

Fig. 1. Details of full-scale specimen (unit: mm): (a) elevation view and test setup of loading phase I ~ V and VII; (b) test setup of loading phase VI; (c) arrangement of the studs; (d) A-A cross section; (e) C–C cross section; (f) B-B cross section; (g) U-rib butt-welded joint; (h) U-rib bolted joint.

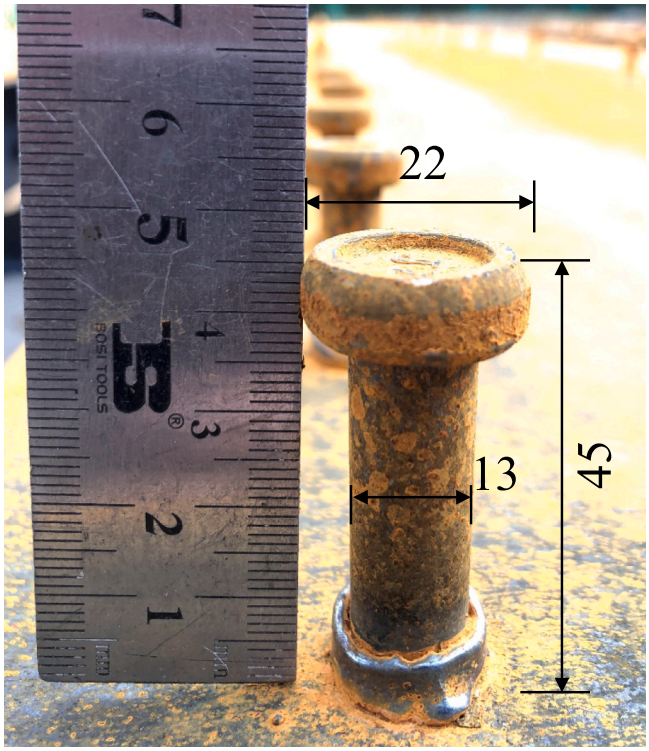

Fig. 2. Details of the short-headed stud connector (unit: mm).

deck. It was found that the local deflection of the OSD was reduced by 45% owing to the contribution of the UHPC layer. Unterweger et al. [19] investigated the strengthening effect of the UHPC layer on the service life of OSD, revealing a 80 mm-thick UHPC layer will guarantee the rib-to-deck plate welded joint and the rib-to-cross beam welded joint at least 50 years in service. Yuan et al. [20] conducted fatigue tests on one OSD specimen before and after casting of a 60 mm-thick rebar reinforced UHPC layer, proving the no fatigue cracks developed in OSD after strengthening by UHPC layer. Liu et al. [21] reported that the UHPC cracks and studs fracture accelerated the fatigue damage of the rib-to-deck and cross beam welded joint of OSD-UHPC composite deck with large-size U-ribs. Chen et al. [22] conducted fatigue test on OSD-UHPC composite deck under negative bending. It is revealed that fatigue damage occurred at the rib-to-crossbeam welded joint firstly, then the OSD-UHPC interface delamination happened, while the UHPC layer exhibited slight fine cracks and did not influence the global performance of the deck system. Feng et al. [18] reported that the rib-to-cross beam welded joint of the composite deck was still vulnerable to fatigue cracks.

The existing studies mainly focused on the stiffening effect of UHPC on the fatigue-prone details of OSD, and the fatigue failure process of the composite deck system. However, researches on the fatigue performance of U-rib butt-welded joint and U-rib bolted joint of the OSD-UHPC composite deck haven't been reported. Furthermore, investigations on the shear fatigue performance of the short-headed stud connectors in the beam fatigue test are still limited. The shear fatigue behavior and the arrangement of the short-headed stud connectors govern the global fatigue resistance of the composite deck system. Therefore, the relevant fatigue behavior evaluation of the composite deck system also needs to be specified. Besides, considering the UHPC layer is reinforced by the rebar mesh, it still deserves to discuss whether it is reasonable to apply the tensile *S-N* curves of UHPC material to evaluate the fatigue performance of the UHPC layer of the composite deck directly.

The objective of this study is to reveal the fatigue damage process and establish *S-N* curves for fatigue behavior evaluation of the OSD-UHPC composite deck system. A two-span full-scale OSD-UHPC composite deck was designed and tested under fatigue loading. Based on this test results and existing researches, the *S-N* curves of the fatigue-prone details of OSD, including the rib-to-cross beam welded joint, the U-rib butt-welded joint and the U-rib bolted joint, and of the short-headed stud connectors were established. The tensile fatigue *S-N* curves of UHPC at three levels, i.e., the material level, the structural member level and the structural system level, were summarized and discussed to evaluate the fatigue cracking resistance of the UHPC layer. The method to evaluate the global fatigue behavior of the composite deck system was suggested.

2. Experimental description

2.1. Specimen design

Fig. 1 shows the details of the full-scale two-span OSD-UHPC composite bridge deck specimen. The length, width and height of the specimen were 8800 mm, 1440 mm and 392 mm, respectively. The OSD consisted of a 12-mm-thick steel deck plate, two 8-mm-thick U-shaped ribs (U-ribs), three cross beams with web thickness of 12 mm and flange plate thickness of 16 mm. The U-ribs had top opening width of 360 mm, bottom width of 240 mm and depth of 300 mm. To compare the fatigue resistance of the U-rib butt-welded joint and the U-rib bolted joint, the two U-ribs at the location of 1000 mm to middle cross beam in longitudinal direction were disconnected, and were connected by butt-welded joint with backing strip and M22 grade high-strength bolts joint, respectively. Hence, the two U-ribs were named as U_w and U_b (w denotes weld, b denotes bolt), and the related details of the two connections were shown in Fig. 1(g) and Fig. 1(h). The UHPC layer was 80 mm thick and was reinforced by φ16 mm rebar mesh at spacing of 200 mm both in longitudinal and transverse directions. The OSD and the top UHPC layer were integrated through the short-headed stud connectors which were welded on the steel deck plate. The short-headed stud connectors were arranged at spacing of 360 mm both in longitudinal and transverse directions, as shown in Fig. 1(c). The stud rows and columns were defined as the numbers of stud connectors in transverse and longitudinal direction, respectively. Hence, the stud rows and stud columns were 5 and 11 respectively in each span. In addition, Fig. 2 plots the details of single stud connector which had diameter of 13 mm and height of 45 mm after welding.

2.2. Specimen fabrication and material properties

Fig. 3 shows the four main fabricating procedures of the specimen. The OSD was firstly made, followed by the welding of short-headed stud connectors to the steel deck plate. Then the rebar mesh and wooden formwork of UHPC layer were arranged. The next procedure was casting and leveling of UHPC layer. To minimize the water evaporation and prevent the shrinkage cracking of UHPC layer, the UHPC layer was covered with plastic sheet as soon as it was leveled. Finally, the UHPC layer was sprinkled and cured under natural curing conditions. After the UHPC layer was cured at least 28 days, the fatigue test could be conducted.

The OSD, stud connector and rebar were made of Q345q steel [23], ML15 [24] and HRB400 [25], respectively. On the basis of the tensile test [26], the mechanical properties of steel, including the modulus of elasticity, yield strength and ultimate strength, are summarized in Table 1.

The UHPC used was a commercial UHPC containing coarse aggregates (CA-UHPC). The specific material compositions of UHPC are shown in Table 2. The 20 mm × 0.25 mm (length × diameter) and 13 mm × 0.2 mm (length × diameter) steel fibers were used to improve the tensile strength and toughness of UHPC. Fig. 4 shows the tests for obtaining the mechanical properties of UHPC. Referring to Chinese Standard CECS13 [27], the specimen sizes of cubic compressive strength test, elastic modulus test, axial compressive strength test and four-point bending test were 100 mm × 100 mm × 100 mm, 100 mm × 100 mm ×

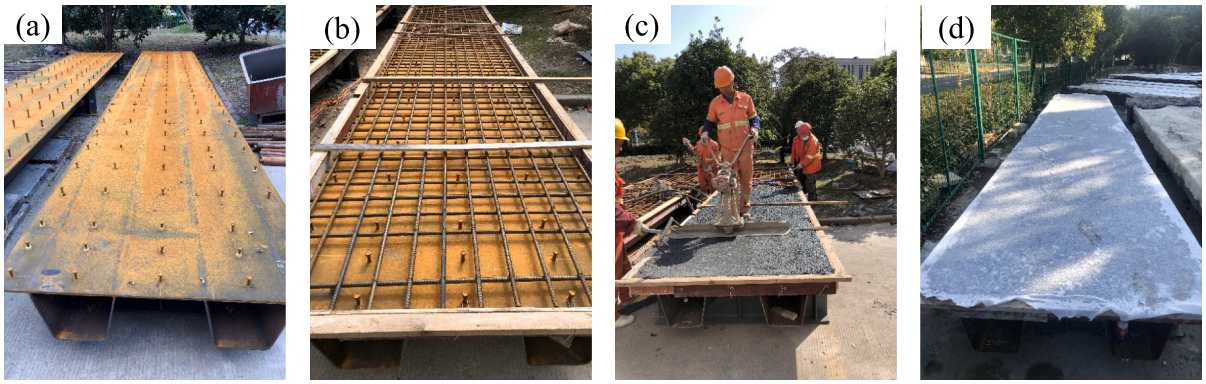

Fig. 3. Specimen fabricating procedures: (a) making of OSD and studs; (b) arranging of rebar mesh and formwork; (c) casting of UHPC layer; (d) curing of UHPC layer.

Table 1
Mechanical properties of steel.

Material	*t* or *d* (mm)	Yield strength (MPa)	Ultimate strength (MPa)	Elastic modulus (GPa)
Q345q	8	411	554	210
	12	370	511	210
HRB400	16	549	664	200
ML15	13	332	479	206

Notes: *t* and *d* refer to thickness and diameter, respectively.

300 mm, 100 mm × 100 mm × 300 mm, and 100 mm × 100 mm × 400 mm, respectively. The direct tensile test (DTT) was designed according to Swiss recommendation [12]. The specimen size of DTT is shown in Fig. 4(c). The material specimens were cured under the same natural curing condition for 28 days with the composite deck specimen. The corresponding mechanical properties of UHPC are summarized in Table 3. It should be noted that the values presented are the mean value of three identical specimens.

2.3. Instrumentation

Fig. 5 shows the instrumentation of the specimen. Laser displacement meter was used to capture the vertical displacement of the mid-span section of the load span. Strain gauges were glued to the surface of the OSD to measure the strain variation. The strain gauges of U-rib-to-deck-plate-to-middle-crossbeam welded joint (U_b-D, U_w-D) were placed at 8 mm distance from the weld root to capture the transverse strain. The strain gauges of the U-rib-to-cross beam welded joint, marked as U_b-MC, U_w-MC, U_b-EC and U_w-EC, were placed at 8 mm distance from the weld toe to capture the vertical strain. The strain variation and potential cracks around the cutouts of the middle cross beam were detected by strain gauges MC-1 ~ MC-6. The longitudinal strain variation of the U-rib butt-welded joint was measured by strain gauges W1 ~ W4 attached on the outer surface of the U-rib bottom flange. The corresponding strains of the U-rib bolted joint were measured by strain gauges B1 ~ B5 glued to splicing plate-4 (sp4 in Fig. 1[f]), and B6 ~ B9 glued to the rib wall. In addition, the global response of the specimen was captured by

Table 3
Mechanical properties of UHPC.

E_c(MPa)	f_c(MPa)	f_{cu}(MPa)	f_{ct} (MPa)	$f_{cr,fl}$(MPa)	$f_{ct,fl}$(MPa)
48,733	96	108	7.45	11.53	22.38

Notes: E_c, f_c, f_{cu}, f_{ct}, $f_{cr,fl}$, $f_{ct,fl}$ denote modulus of elasticity, axial compressive strength, cubic compressive strength, tensile strength, first cracking strength under flexural tension and flexural strength, respectively.

Table 2
Material compositions of 1 m^3 UHPC.

Item	Reactive powder	River sand	Basalt aggregate	Steel fibers	Superplasticizer	Water
Weight(kg)	1173	616	472	198	25.7	138
Size	micron	4–5 mm	less than8mm	hybrid	—	—

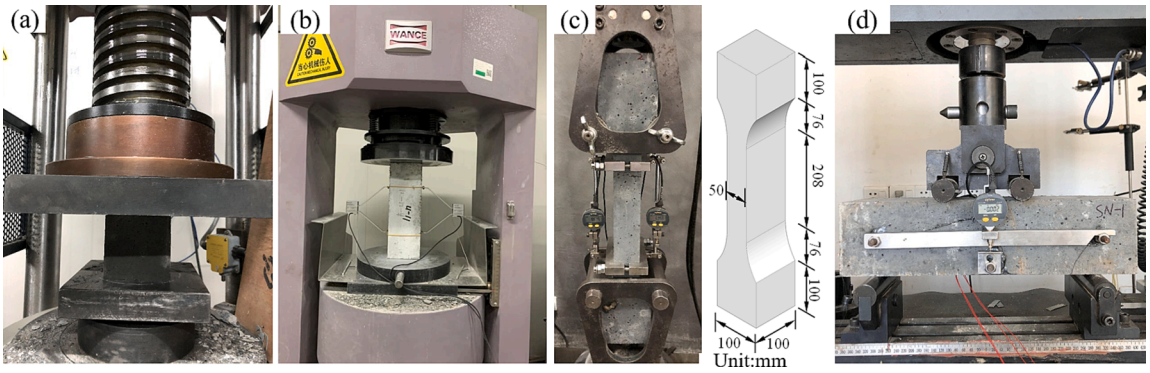

Fig. 4. Mechanical properties tests of UHPC: (a) cubic compressive strength test; (b) elastic modulus and axial compressive strength tests; (c) direct tensile test; (d) four-point bending test.

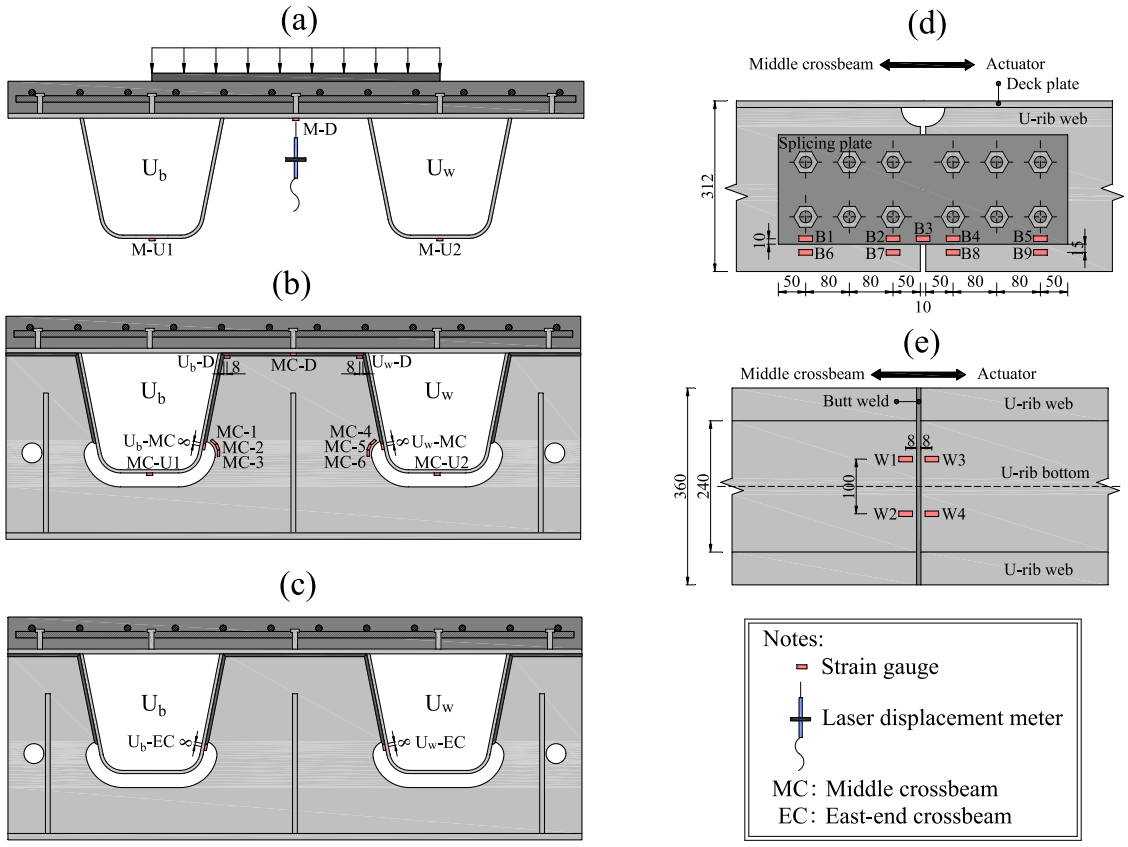

Fig. 5. Instrumentation of specimen (unit: mm): (a) mid-span section of loading span; (b) section at the middle cross beam (MC); (c) section at the east-end cross beam (EC); (d) U-rib bolted joint; (e) U-rib butt-welded joint.

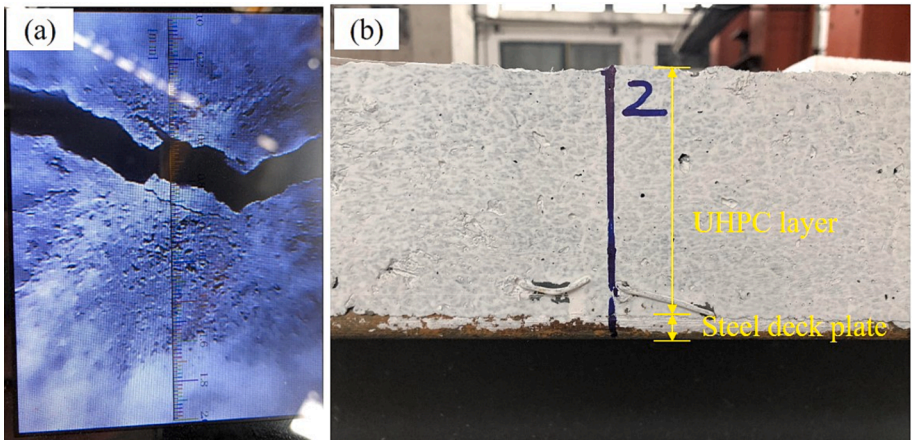

Fig. 6. Instrumentation of specimen: (a) crack observer; (b) The marked interface at 2-N.

longitudinal strain gauges on the bottom surfaces of the steel deck plate and of the U-ribs, at the mid-span section as well as the section at the middle cross beam.

The crack width changes of the UHPC layer above the middle cross beam were captured by crack observer with an accuracy of 0.01 mm, as shown in Fig. 6(a). The shear fatigue fracture of short-headed stud connectors was defined as interface debonding at the marked OSD-UHPC interfaces at the side edges, as shown in Fig. 1(c) and Fig. 6(b). Take the mark "2-N" as an example, it stands for the OSD-UHPC interface locating in the second stud column at the north-side edge.

2.4. Test setup and loading protocol

Fig. 1(a), Fig. 1(b) and Fig. 7 show the test setup. The specimen was fixed and supported by three steel pedestals which were attached to the ground using high-strength cement mortar. The hydraulic actuator was placed at the mid-span section of the load span, and the cyclic load was enforced to the specimen through a spreader beam. A rubber gasket with length, width and thickness of 720 mm, 200 mm and 20 mm respectively, was installed between the spreader beam and the UHPC layer to simulate the effect of the vehicle wheel load. To avoid vibration of no-load span (the span from middle cross beam to west-end cross beam),

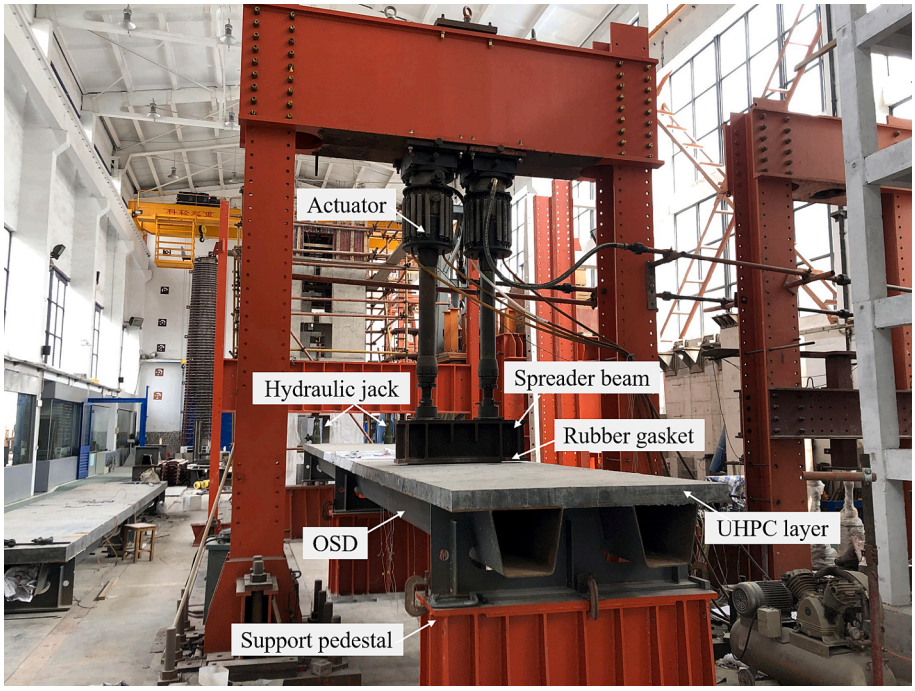

Fig. 7. Test setup.

Table 4
Fatigue loading protocol.

Phase	Style	Load level P_{min} ~ P_{max} (kN)	Load amplitude ΔP (kN)	Strss range of UHPC layer (MPa)	Cyclic Numbers N_i ($\times 10^4$)	Loading frequency (Hz)
I	Cyclic	271 ~ 405	134	2.90	200	4
II	Cyclic	310 ~ 539	229	4.96	100	4
III	Cyclic	560 ~ 807	247	5.35	160	4
IV	Cyclic	798 ~ 1075	277	5.99	40	4
V	Cyclic	421 ~ 730	309	6.69	50	4
VI	Static	400	—	—	—	—
VII	Cyclic	505 ~ 730	225	4.87	100	4

two hydraulic jacks were installed between the rear reaction frame (above the west-end cross beam) and the specimen.

Table 4 shows the loading protocol. According to the prototype bridge design [28], the tensile stress of UHPC layer at the negative moment zone under dead load and traffic live load was approximately 5.85 MPa and 2.90 MPa, respectively. So the minimum load P_{min} and the load amplitude ΔP at loading phase I were 270 kN (corresponding to 5.85 MPa) and 134 kN (corresponding to 2.90 MPa), respectively. The cyclic loading phase I was designed to assess the fatigue performance of the OSD-UHPC composite deck in design service life during which the fatigue life is reaching 2 million cycles. The rest loading phases were to determine the fatigue damage process and degradation of mechanical

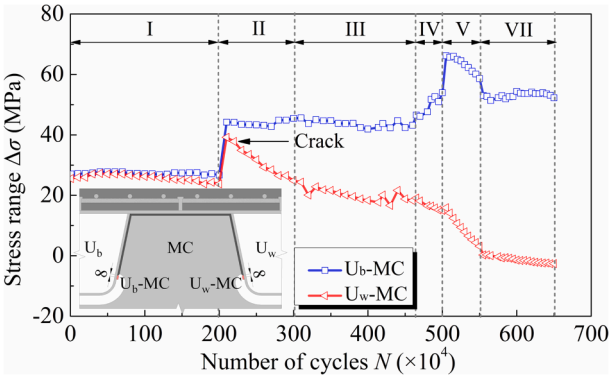

Fig. 9. Stress range evolution of measuring points at the rib-to-middle cross beam welds.

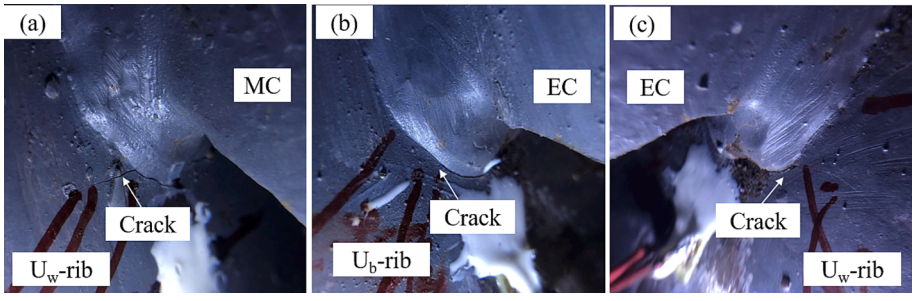

Fig. 8. Crack at the rib-to-cross beam welded joint (MC: middle cross beam, EC: east-end cross beam).

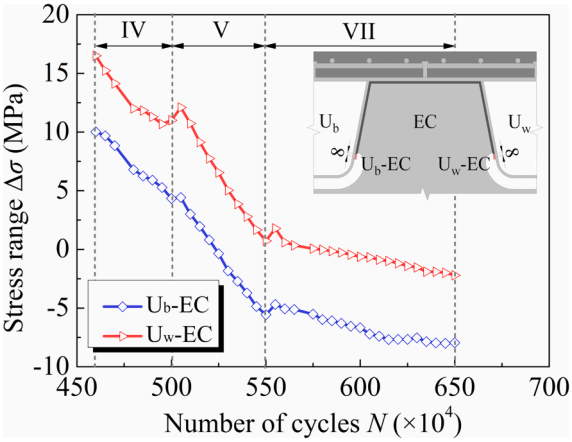

Fig. 10. Stress range evolution of measuring points at the rib-to-east-end cross beam welds.

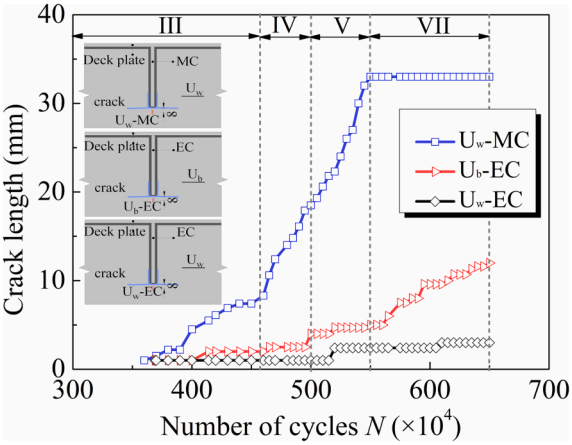

Fig. 11. Length evolution of longitudinal cracks at the rib-to-cross beam welds.

properties of the composite deck by increasing the load amplitude. It should be noted that cyclic loading phase I ~ V were based on the two-span continuous test setup shown in Fig. 1 (a). The static loading phase VI was based on the simply-supported cantilever test setup shown in Fig. 1 (b). This phase was to make the UHPC layer above the middle cross beam develop more cracks and make the maximum crack width reach up to 0.2 mm. In practice of phase VI, the UHPC maximum crack width of only 0.15 mm was achieved under the static maximum load of 400 kN considering the loading safety of the specimen. The cyclic loading phase VII was still based on the two-span continuous test setup shown in Fig. 1 (a), and this phase was to investigate the fatigue performance of the composite deck after the UHPC layer suffered from severe pre-cracking in the static loading phase VI. The loading frequency was kept constant at 4 Hz during the cyclic loading phases. To investigate the stiffness degradation of the specimen, the static tests were conducted before and during the cyclic loading phases. The static test was applied to the maximum load of the corresponding cyclic loading phases every 50,000 cycles.

3. Test results and analysis

3.1. Fatigue damage process

3.1.1. OSD

In loading phase I after 2 million cycles, there were no fatigue cracks observed at the fatigue-sensitive details on the OSD, indicating that the

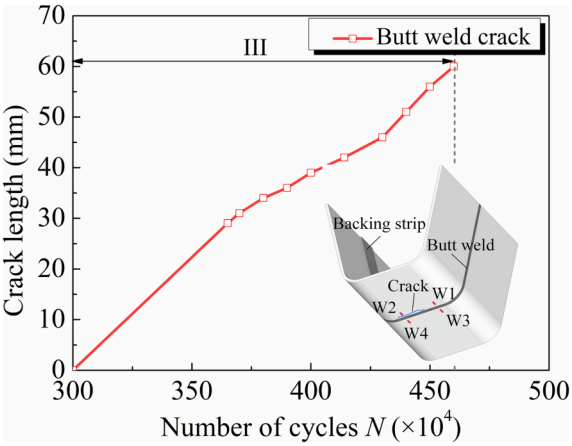

Fig. 13. Length evolution of crack at the U-rib butt-welded joint.

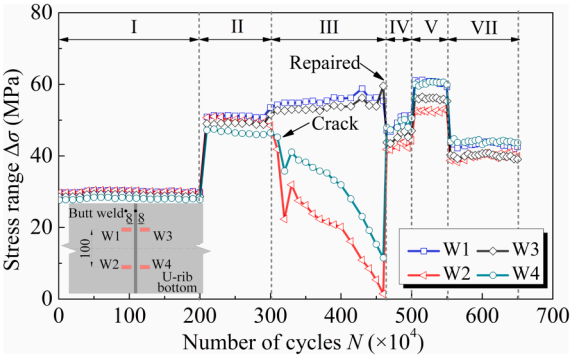

Fig. 14. Stress range evolution of measuring points at the U-rib butt-welded joint.

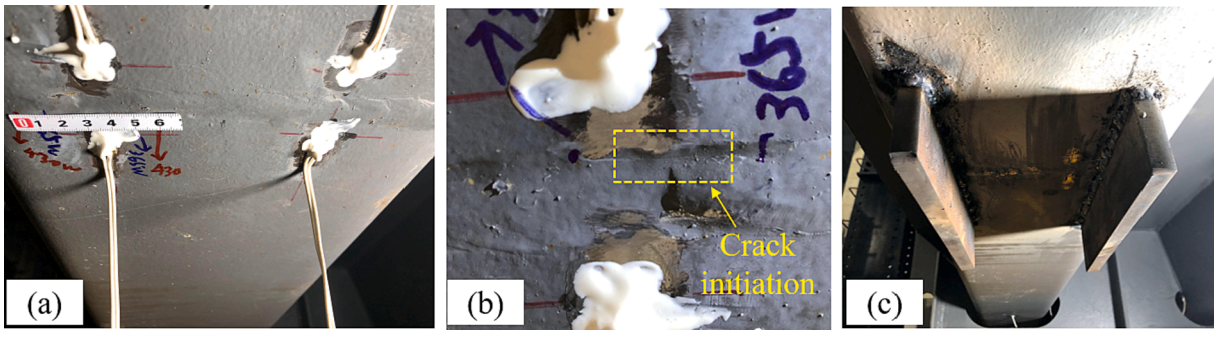

Fig. 12. The U-rib butt-welded joint: (a) fatigue crack; (b) welding defects; (c) repairing and stiffening scheme.

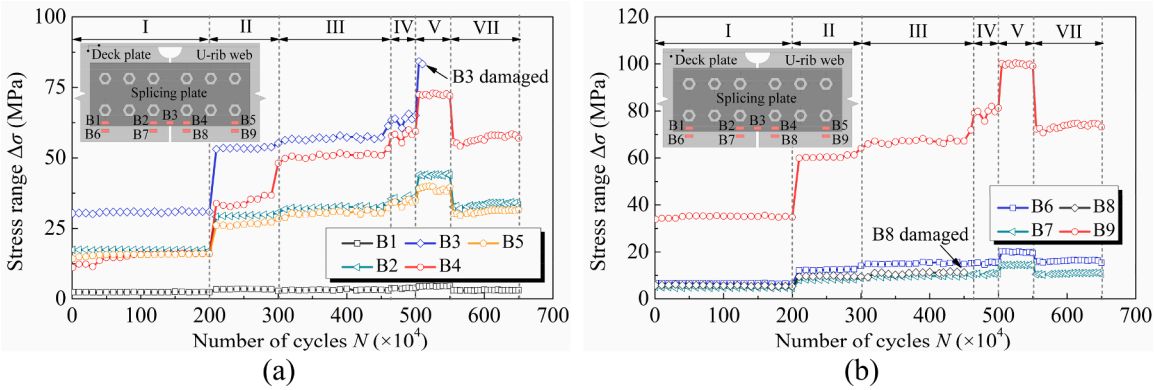

Fig. 15. Stress range evolution of measuring points at the U-rib bolted joint: (a) splicing plate; (b) U-rib.

Fig. 16. Interface debonding at 3-N.

Table 5
Test results of the short-headed stud connectors.

Number	N_f (×10^4)	$\Delta\tau_e$ (MPa)	Number	N_f (×10^4)	$\Delta\tau_e$ (MPa)
3-N	405	187.9	4-S	498	198.9
2-S	414	188.7	5-N	539	211.4
2-N	420	189.2	10-S	525	142.2
1-N	429	189.9	8-N	539	144.7
1-S	429	189.9	8-S	539	144.7
3-S	429	189.9	9-N	539	144.7
0-N	481	196.1	9-S	539	144.7
0-S	491	197.8	10-N	549	146.2

fatigue performance of the OSD in the OSD-UHPC composite deck specimen satisfies the design requirement. Fatigue crack was firstly observed at the lowest location of the U_w-rib-to-middle cross beam welds at 2.06 million cycles. The crack initiated at the weld toe at the U_w-rib side and propagated upward along the weld toe until the vertical crack length reaching 41 mm at 3.65 million cycles. Then the vertical crack stopped growing, and the longitudinal crack started to propagate on the U_w-rib wall in longitudinal direction. Fig. 8 shows the crack close to the U_w-rib-to-middle cross beam welded joint. The initiation of the fatigue crack could be reflected by the stress range variation of the measuring points below the weld toe, as plotted in Fig. 9. As shown, the stress range of strain gauge U_w-MC started to decline at about 2.1 million cycles which was close to the time of visual observation of cracking at 2.06 million cycles. The reason for stress drop was the stress relief caused by local cracking. It is clear that the stress ranges of strain gauge U_b-MC were kept almost constant at each loading phase, indicating no fatigue cracks occurred at the weld.

Fatigue cracks close to the rib-to-east-end cross beam welded joint were also observed at 3.69 million cycles, as shown in Fig. 8. The monitoring strain gauges U_b-EC and U_w-EC (shown in Fig. 5 [c]) were installed at the end of the loading phase III. The corresponding response of stress range against cyclic numbers is plotted in Fig. 10. As shown, the stress ranges of the two measuring points exhibited a descending trend from phase IV to the end of the fatigue test.

Fig. 11 shows the length propagation of longitudinal cracks at the rib-to-cross beam welded joint. The crack at the U_w-rib-to-middle cross beam welded joint developed relatively low in phase III, and developed faster from phase IV to phase V due to the larger load ranges. The crack length was kept at 33 mm during the last loading phase. The two cracks at the rib-to-east-end cross beam welded joint propagated slower than that at the rib-to-middle cross beam welded joint because of the lower stress in east-end cross beam. The length of the two cracks reached 2 mm and 3 mm respectively at the end of fatigue test.

A 29-mm-long crack along the U-rib butt-welded joint at the bottom flange of U_w-rib was observed at 3.65 million cycles. Fig. 12 shows the crack at the U-rib butt-welded joint. The crack initiated from the butt weld with welding defects in which the weld exhibited crater compared with the adjacent full weld, as shown in Fig. 12 (b). As plotted in Fig. 13, the crack length propagated at a constant rate in phase III. In order to ensure the fatigue test could be normally conducted in the following phases, the cracked butt-weld was repaired by penetration welding and the related bottom flange was stiffened by two 16-mm-thick steel plates through welding at the end of phase III. The repairing and stiffening scheme is shown in Fig. 12 (c). Fig. 14 plots stress range evolution of measuring points near the butt weld. As plotted, the stress ranges of measuring points W2 and W4 dropped obviously at 3 million cycles, while that of W1 and W3 presented a slight climbing trend at the same time. It could be presumed that the crack initiated at 3 million cycles. As shown in Fig. 12 (b), the measuring points W2 and W4 were close to the initiating point of the fatigue crack. After the crack was strengthened from phase IV, the stress ranges of all measuring points stayed relatively constant until the end of the fatigue test, proving the effectiveness of the repairing and stiffening scheme.

No fatigue cracks were observed at the U-rib bolted joint. The stress range evolution of measuring points at the bolted joint are plotted in Fig. 15. As shown, the stress ranges of measuring points were kept almost equal at each cyclic loading phase, indicating that no severe fatigue damage occurred at the bolted joint. The U-rib bolted joint exhibited much better fatigue resistance than the U-rib butt-welded joint under the identical loading conditions. Therefore, the bolted joint is recommended as the connecting method for U-ribs when installed on site considering the excellent fatigue resistance of the bolted joint and the common welding defects of the butt-welded joint.

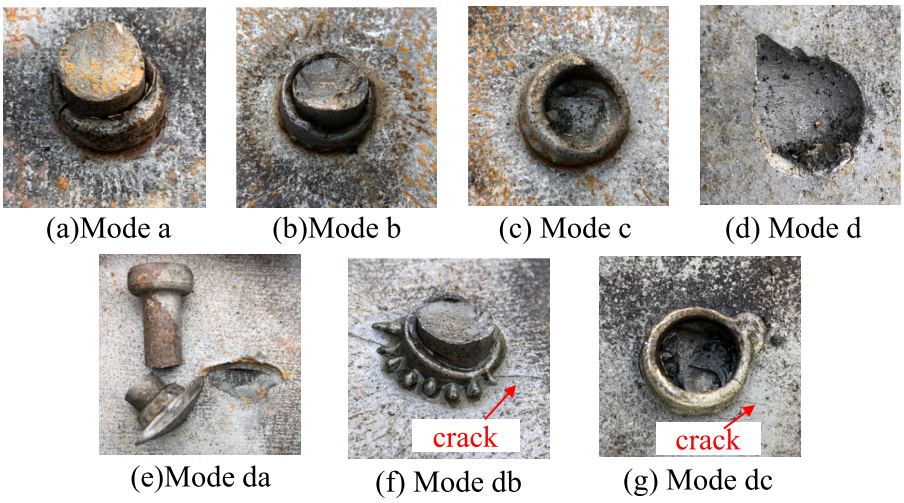

Fig. 17. Fatigue failure modes of the short-headed stud connectors and the steel deck plate.

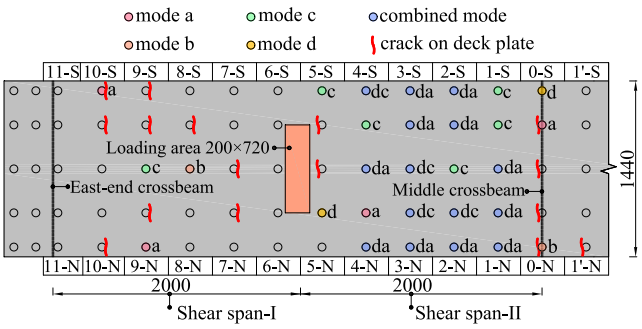

Fig. 18. Distribution of fatigue failure modes (unit: mm).

3.1.2. Short-headed stud connectors

The first visible interface debonding between the OSD and the UHPC layer occurred at the 3-N interface at 4.05 million cycles, as shown in Fig. 16. The obvious vertical debonding and longitudinal slippage could be felt by finger touching on the interface. Then the marked interfaces occurring debonding came to increase with the increase of the cycles. Table 5 lists the interfaces occurring debonding and the corresponding fatigue life (number of cycles that debonding occurred). As shown, the debonding interfaces were located at the load span.

To observe the fatigue failure modes of the short-headed stud connectors, the UHPC layer was removed by high-pressure water jet after completion of the fatigue test. The failure modes could be classified into 5 types, mode a ~ d and combined mode da, db and dc, as shown in Fig. 17. More detailed fatigue failure modes and failure mechanism could be found in literature [28]. The distribution of fatigue failure modes is shown in Fig. 18. As shown, the short-headed stud connectors and the steel deck plate occurring fatigue damage are located at the load span, and the fractured stud connectors are located at the shear span-II at which the stud connectors suffered from higher shear stress range. Besides, the fractured stud connectors were almost aligned with the interfaces occurring debonding listed in Table 5, indicating the feasibility of judging fatigue fracture of the stud connectors by visual observation of interface debonding.

Assuming that the shear force at the interface was uniformly shared by all the short-headed stud connectors at the same shear span, the nominal shear stress range of the short-headed stud connectors can be derived as:

$$\Delta\tau = \frac{\Delta V S_0 L(x)}{I_0 n_1 n_2 A_{sd}} \tag{1}$$

where: ΔV is shear force range; I_0 is the moment of inertia of the composite section; S_0 is the area moment of concrete section to the center of gravity axis of the composite section; $L(x)$ is the length of shear span; A_{sd} is the cross-section area of stud shank; n_1 is number of stud rows; n_2 is number of stud columns.

A variable amplitude shear force was enforced to the short-headed stud connectors during the loading phases. The equivalent constant amplitude shear stress range at the fatigue life can be obtained according to the linear damage cumulative theory [29]:

$$\Delta\tau_e = \left[\frac{\sum N_i(\Delta\tau_i)^m}{N_f}\right]^{1/m} \tag{2}$$

where $\Delta\tau_e$ is the equivalent constant amplitude nominal shear stress range; N_f is the fatigue life ; $\Delta\tau_i$ is the shear stress range at each loading phase; N_i is cyclic numbers corresponding to $\Delta\tau_i$; m is material constant ($m = 8$ according to Eurocode 4 [30]). The calculated equivalent constant amplitude shear stress ranges against the fatigue life are listed in Table 5.

3.1.3. UHPC layer

Fig. 19 shows the crack distribution on the top surface of the top UHPC layer under the maximum load from phase V to phase VII. As shown, nine discrete cracks were observed above the middle cross beam in phase I, and the maximum crack width was 0.02 mm which was almost the thinnest crack width that could be captured by visual observation. The cracks of UHPC layer exhibited a limited propagation from phase I to phase V, and the maximum crack width was only 0.04 mm under the maximum load at the end of phase V. In the static loading phase VI based on the simply-supported cantilever test setup shown in Fig. 1 (b), multiple transverse continuous cracks appeared on the UHPC layer under the maximum static load of 400 kN. The cracking spacing varied from 75 mm to 120 mm, and the maximum crack width was up to 0.15 mm. Most cracks were closed when the loading phase transformed from static loading phase VI (based on the simply-supported cantilever test setup) to cyclic loading phase VII (based on the two-span continuous test setup). As shown in Fig. 19 (c), only 7 transverse continuous cracks emerging in phase VI remained under the maximum cyclic load of phase VII, and the maximum crack width was 0.04 mm. It is clear that the UHPC cracks emerging in static loading phase VI were still in elastic stage and didn't suffer from severe plastic damage.

According to the research of Rafiee [31], the UHPC behaves as a

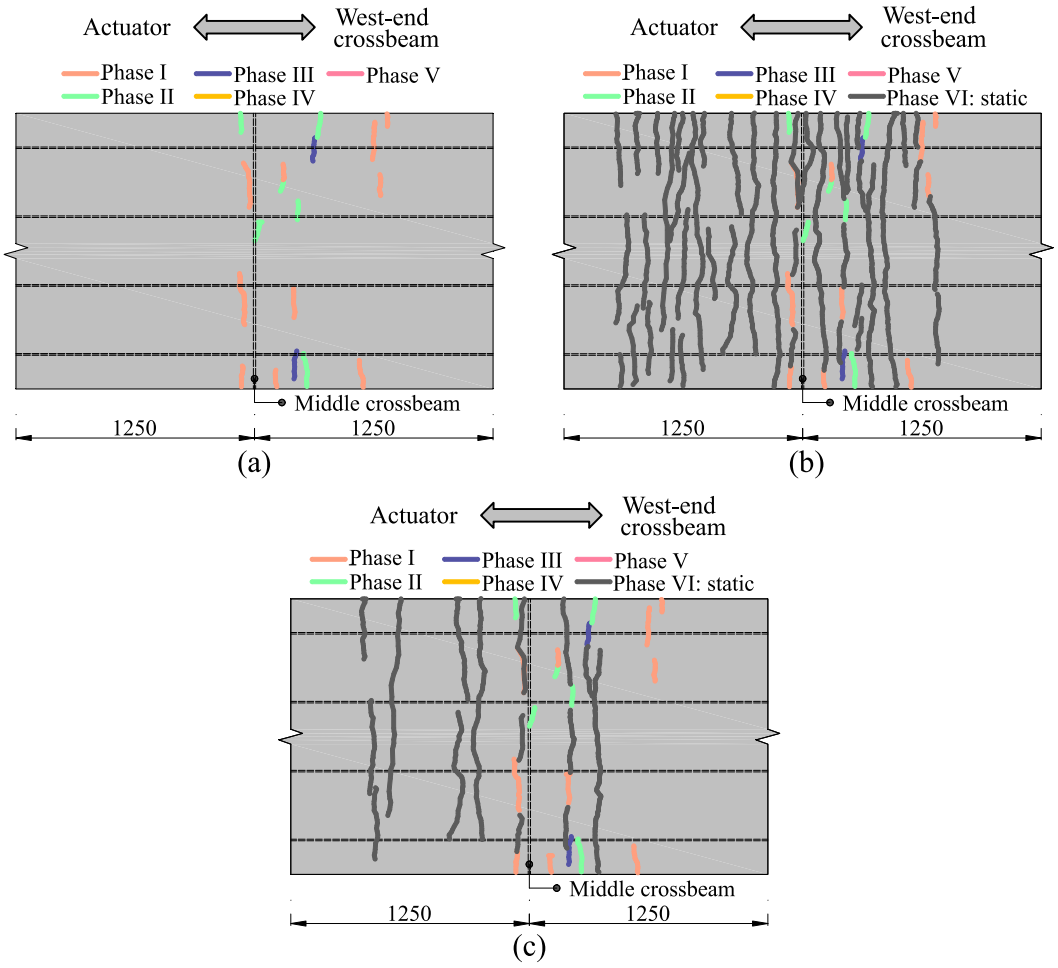

Fig. 19. Crack distribution on the top surface of UHPC layer under the maximum load (unit: mm): (a) in phase V; (b) in phase VI; (c) in phase VII.

sound concrete when the crack width is less than 0.05 mm from the viewpoint of durability. In this view, the maximum crack width of the UHPC layer was 0.04 mm after experiencing 6.5 million cycles of cyclic loading, which meets the critical crack width of durability. In general, the rebar reinforced UHPC layer exhibited excellent anti-fatigue cracking capacity, and the UHPC layer didn't sustained serious fatigue damage considering both the crack numbers and the maximum crack width. In other words, the UHPC layer could still provide sufficient stiffening effect for the composite deck system even after experiencing enlarged cyclic loads in this study.

3.1.4. *Summary of fatigue damage process*

Based on the above observations, the fatigue damage process of the OSD-UHPC composite deck specimen is listed in Table 6. The rib-to-cross beam welded joint was the most fatigue-sensitive detail of the OSD. The fatigue crack on the U-rib initiated at the lowest part of the weld toe at 2.06 million cycles and propagated to each side of the U-rib. Then fatigue crack at U-rib butt-welded joint developed at 3 million cycles. The OSD-UHPC interface deboning firstly happened at 4.05 million cycles. During the whole loading phases, the UHPC layer exhibited excellent anti-fatigue cracking capacity considering the crack numbers and the maximum crack width less than 0.05 mm.

Considering that the OSD-concrete composite deck is a newly developed deck system compared with the traditional OSD, the fatigue damage process of full-scale fatigue test for the composite deck in existing literatures [18,21,22,32–35] is summarized in Table 6. Not only UHPC, but also normal concrete (NC) and engineered cementitious composites (ECC) were applied as the concrete layer in the application practice of the composite deck system.

As illustrated in Table 6, the fatigue damage process of the OSD-concrete composite deck system depends on both the material properties and geometric properties of the structural members, including the concrete material, the thickness of the concrete layer, the reinforcement ratio, the stud spacing and the fatigue-sensitive details of OSD. In general, the rib-to-cross beam welded joint is the most fatigue-sensitive detail. The OSD-concrete interface debonding is determined by the spacing of the stud connectors. No interface debonding happens if the spacing is less than or equal to 225 mm, while that occurs if spacing larger than or equal to 300 mm. In addition, the concrete layer which locates above cross beams cracks under cyclic loading no matter the concrete material is UHPC, ECC or NC. But the maximum crack width is less than 0.1 mm. The cracked concrete layer has a negligible effect on the fatigue performance of the composite deck, and this has been validated in literature [18,22,32,34].

3.2. *Response of global mechanical properties*

3.2.1. *Stiffness degradation*

The global flexural stiffness degradation could be reflected by the load-midspan deflection response under static loading after specific numbers of cyclic loading. Fig. 20 plots the load-midspan deflection response. It is clear that the curves at different cyclic numbers are almost coincided, indicating that the stiffness degradation of the specimen is insignificant. Regarding the fatigue damage, the longitudinal crack

Table 6
Fatigue damage process of the OSD-concrete composite deck.

Ref.	Steel deck	Stud spacing	Concrete layer	Damage process
[32]	14 mm	525 × 400 mm	NC-150 mm-0.6%	2.00 million, NC layer, w = 0.08 mm 2.50 million, interface debonding 2.98 million, detail 1
[34]	12 mm	225 × 225 mm	ECC-85 mm-1.2%	0.20 million, ECC layer, w = 0.04 mm 7.40 million, detail 2
	12 mm	225 × 225 mm	ECC-85 mm-1.2%	0.10 million, ECC layer, w = 0.03 mm
[21]	12 mm	225 × 225 mm	UHPC-60 mm-1.8%	0.20 million, UHPC layer, w = 0.03 mm 5.20 million, detail 1 9.70 million, UHPC layer, w = 0.1 mm
[33]	12 mm	225 × 225 mm	UHPC-60 mm-1.8%	0.20 million, UHPC layer, w = 0.05 mm 5.20 million, detail 1 9.00 million, UHPC layer, w less than 0.09 mm
[18]	16 mm	150 × 150 mm	UHPC-50 mm-1.8%	1.14 million, detail 1 3.23 million, detail 4 5.29 million, UHPC layer, w = 0.05 mm
[35]	12 mm	300 × 310 mm	UHPC-45 mm-3.6%	2.75 million, detail 3 3.00 million, detail 2
[22]	16 mm	300 × 300 mm	UHPC-45 mm-1.7%	3.62 million, detail 1 5.31 million, interface debonding 6.00 million, UHPC layer, slight fine cracks
	16 mm	300 × 300 mm	UHPC-45 mm-1.7%	2.20 million, detail 1 4.10 million, interface debonding 5.00 million, UHPC layer, slight fine cracks
	16 mm	300 × 300 mm	UHPC-45 mm-2.5%	0.25 million, detail 1 1.11 million, interface debonding 2.00 million, UHPC layer, slight fine cracks
	16 mm	300 × 300 mm	UHPC-45 mm-2.5%	0.39 million, detail 1 1.60 million, interface debonding 2.83 million, UHPC layer, slight fine cracks
This study	12 mm	360 × 360 mm	UHPC-80 mm-2.0%	2.06 million, detail 1 3.00 million, detail 3 4.05 million, interface debonding 6.50 million, UHPC layer, w = 0.04 mm

Notes: "Steel deck" refers to the thickness of the steel deck plate, "Stud spacing" refers to longitudinal spacing × transverse spacing, "Concrete layer" refers to concrete type-thickness of concrete layer-reinforcement ratio, w refers to the maximum crack width of the concrete layer. Detail 1 to 4 refer to crack at the rib-to-cross beam weld, crack at the rib-to-steel deck plate weld, crack at the U-rib butt-welded joint and crack at the cross-beam cutout, respectively.

(with final length of 33 mm) at the rib-to-crossbeam welded joint and interface debonding did not make significant contribution to the stiffness degradation. In literature [22], because the longitudinal crack at the rib-to-cross beam welded joint had penetrated into the rib-to-steel deck welded joint, the stiffness of the OSD-UHPC composite deck exhibited a serious decrease.

3.2.2. Stress variation of typical cross sections

The evolution of longitudinal stress range of measuring points at mid-span cross section and middle crossbeam cross section is show in Fig. 21. The stress ranges of typical cross sections stayed almost constant in each cyclic loading phase except from some fluctuation of measuring point MC-D. This indicates that the global mechanical properties of the composite deck are relatively stable in each cyclic loading phase. All in all, the fatigue cracks of the OSD, the interface debonding and the UHPC cracks did not lead to severe degradation of global mechanical properties of the OSD-UHPC composite deck specimen, considering the load-midspan deflection response as well as the stress variation of typical cross sections.

4. Discussion on fatigue behavior evaluation of composite deck system

4.1. Fatigue behavior evaluation of OSD

4.1.1. Rib-to-cross beam welded joint

As mentioned above, the rib-to-cross beam welded joint is the most fatigue-prone cracking detail in the OSD-UHPC composite deck. Fig. 22 shows the three cracking patterns at the rib-to-cross beam welded joint, i.e., the vertical crack on U-rib, the longitudinal crack on U-rib and the crack on cross beam. The AASHTO [36] covers the three cracking patterns which are defined as category C with fatigue strength of 89.7 MP at 2 million cycles. The TB10091 [37] also covers the three cracking patterns, and three patterns are set as category XIIIV with fatigue strength of 45 MP at 2 million cycles. The Eurocode 3 [38] only considers the two cracking patterns on U-rib. For the longitudinal crack on U-rib, the detail is defined as category 80 if the thickness of the cross beam less than or equal to 12 mm, while is defined as category 71 if larger than 12 mm. For the vertical crack on U-rib, the fatigue category depends on the weld length, and is defined as category 56 when the weld length larger than 56 mm.

Because no cracks which initiated at the rib-to-cross beam welded joint and propagated on cross beam were observed in the full-scale fatigue test of OSD-UHPC composite deck [18,21,22,32,33], the fatigue behavior of longitudinal and vertical cracks on U-rib will be discussed as following. The OSD-UHPC composite deck specimen of this test was subjected to a variable amplitude cyclic load. The stress range measured by strain gauge U_w-MC could be used to evaluate the fatigue behavior of the rib-to-cross beam welded joint. The stress range fall of 10% [1] was chosen as the fatigue failure criteria for the rib-to-cross beam welded joint. Based on the linear damage cumulative theory [29], the equivalent constant amplitude stress range at fatigue life can be obtained using the following equation,

$$\Delta\sigma_e = \left[\frac{\sum N_i(\Delta\sigma_i)^m}{N_f}\right]^{1/m} \tag{3}$$

where $\Delta\sigma_e$ is the equivalent constant amplitude stress range; N_f is the fatigue life ; $\Delta\sigma_i$ is stress range at each loading phase; N_i is cyclic numbers corresponding to $\Delta\sigma_i$; m is the slope of S-N curve (m = 3 according to Eurocode 3 [38]).

The fatigue test results, i.e., fatigue life and stress range, of the longitudinal crack on U-rib at the rib-to-cross beam welded joint from both the traditional OSD specimens [1,39–42] and OSD-concrete composite deck [22,32,33] specimens were summarized. Based on these data, the S-N curves with survival probability of 5%, 50% and 95% were obtained according to linear regression analysis recommended by the International Institute of Welding (IIW) [43], as shown in Fig. 23. This test result and the obtained S-N curve with survival probability of 95% were compared with S-N curves of existing design codes, as plotted in Fig. 24. As shown, the obtained S-N curve with 95% survival probability is close to the S-N curve of TB10091. The S-N curve of AASHTO lies above all other curves, and that of Eurocode 3 lies between AASHTO and the obtained. In addition, the test result lies below the S-N curve of TB10091 which is the lowest curve, indicating that the fatigue detail of the specimen did not conform to the fatigue strength of design codes. This could be caused by the welding process and welding defects.

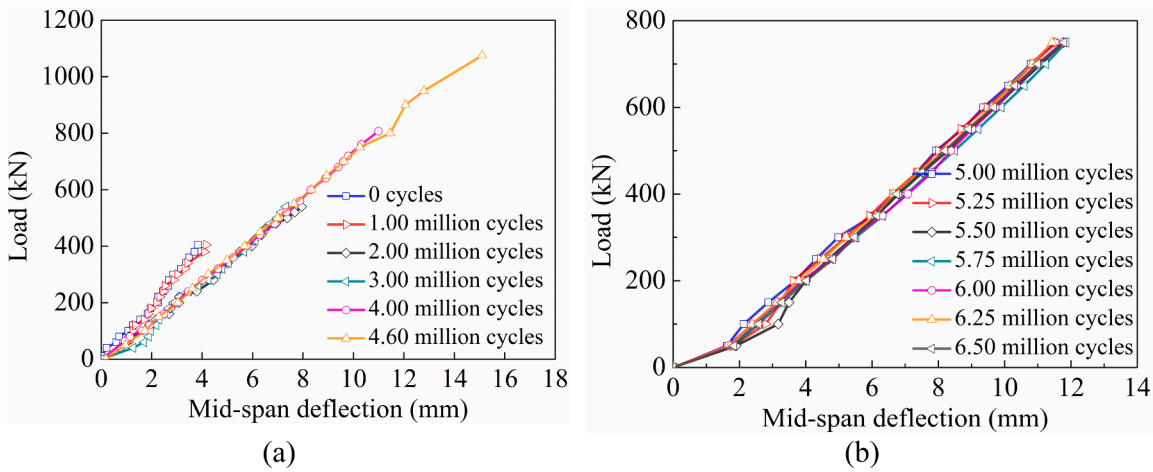

Fig. 20. Load-midspan deflection response.

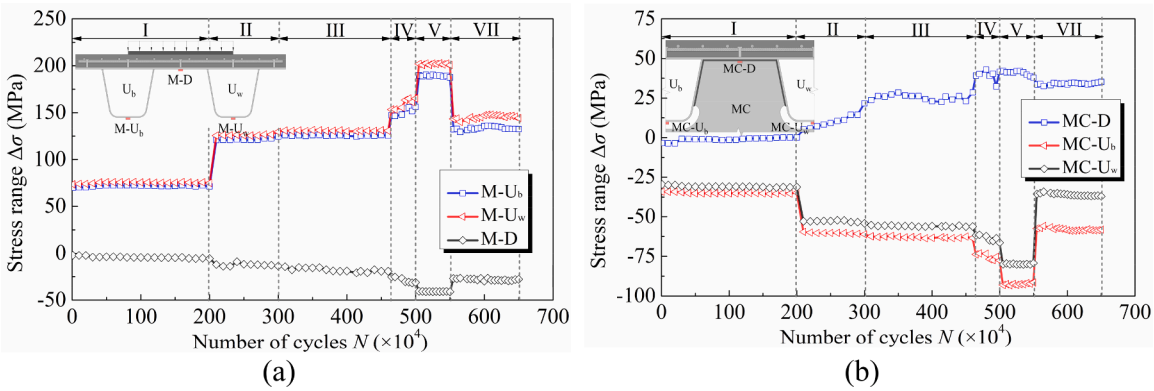

Fig. 21. Evolution of longitudinal stress range: (a) cross section at mid-span; (b) cross section at the middle cross beam.

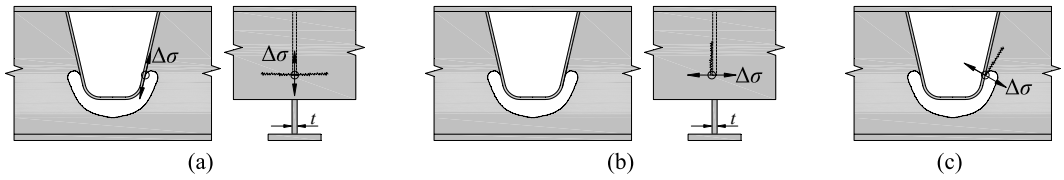

Fig. 22. Fatigue crack at rib-to-crossbeam welded joint: (a) longitudinal crack on U-rib; (b) vertical crack on U-rib; (c) crack on crossbeam.

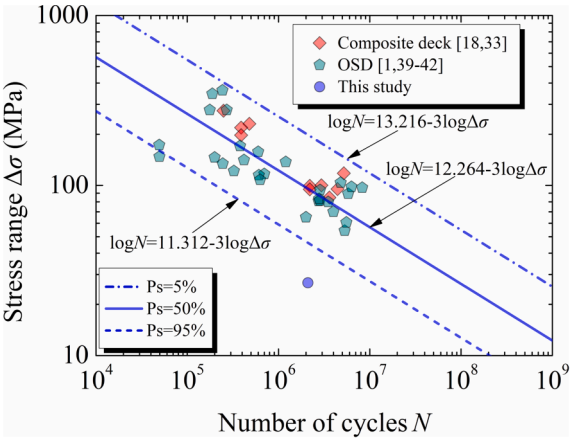

Fig. 23. *S-N* curves of longitudinal crack at the rib-to-crossbeam welded joint.

In this fatigue test, no longitudinal strain gauges were attached to capture the vertical crack on U-rib at the rib-to-cross beam welded joint. This crack was not reported in the relevant full-scale fatigue test of OSD-concrete composite deck [18,21,22,32,33]. The related S-N curves of existing design codes were compared as show in Fig. 24 (b). As shown, the AASHTO [36] has the largest fatigue strength 89.7 MPa at 2 million cycles, which is almost twice of that of TB10091 [37]. The fatigue strength of Eurocode 3[38] lies between the AASHTO [36] and TB10091 [37], and the value is determined by the thickness of the cross beam.

4.1.2. U-rib butt-welded joint

The U-rib butt-welded joint with backing strip is sensitive to fatigue cracking. According to Kondo [44] and Kolstein [1], the fatigue strength of this detail is associated with the size of root gap, as shown in Fig. 25. The fatigue data of the OSD specimens and the OSD-concrete composite deck specimens was classified based on the weld root gap less than 5 mm [1,44] and larger than or equal to 5 mm [1,44–48]. Considering the size of root gap (less than 5 mm, larger than 5 mm, and including all the

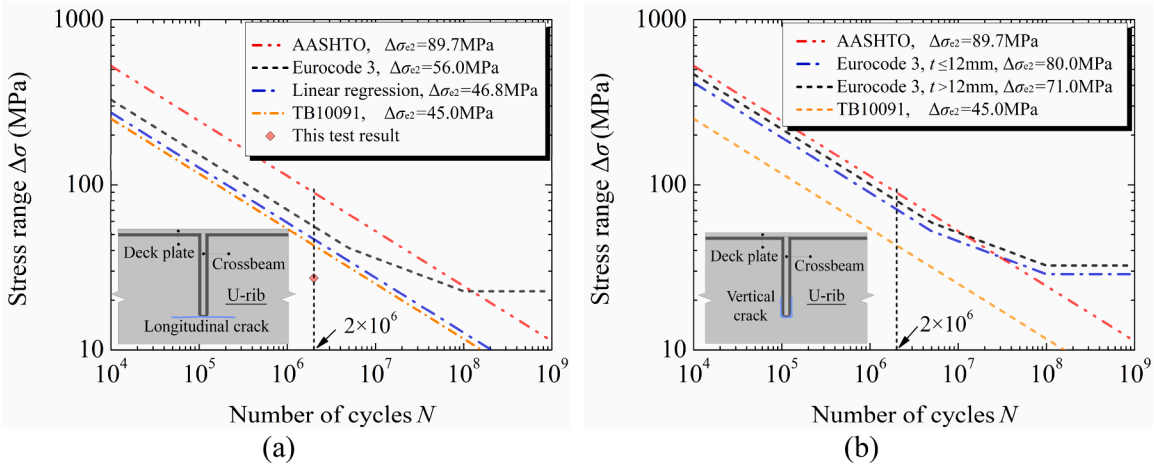

Fig. 24. *S-N* curves comparison with existing design codes: (a) longitudinal crack; (b) vertical crack.

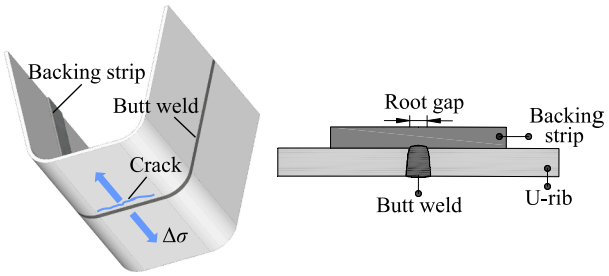

Fig. 25. U-rib butt-welded joint with backing strip.

sizes), the *S-N* curves with survival probability of 5%, 50% and 95% were obtained according to linear regression analysis recommended by IIW [43]. The established *S-N* curves with 95% survival probability were compared with existing design codes, as plotted in Fig. 26.

As shown, the fatigue strength of the U-rib butt-welded joint is considerably influenced by the root gap size. The fatigue strength at 2 million cycles of root gap larger than or equal to 5 mm is 73.5 MPa, which is close to three times as large as that of root gap less than 5 mm. When considering all sizes, the fatigue strength decreases from 73.5 MPa to 36.1 MPa. Furthermore, the fatigue strength of root gap larger than or equal to 5 mm is close to the that of the three design codes. Lastly, the result of this fatigue test lies below the *S-N* curves of the three design codes, indicating the fatigue performance of the U-rib butt-welded joint with backing strip of the specimen did not satisfy the design requirements. This was induced by the initial welding defects which exhibited crater.

4.1.3. U-rib bolted joint

The design philosophy of the U-rib bolted joint is to ensure that the fatigue cracking of the splicing plates occurs no later than the U-rib, for the splicing plates which are more convenient to replace. In this fatigue test, no fatigue cracks occurred on the splicing plates and the U-rib. The test results [47,49] occurring fatigue cracking on the splicing plates in full-scale OSD specimens were summarized, and the *S-N* curves with survival probability of 5%, 50% and 95% were obtained. The established *S-N* curves with 95% survival probability were compared with existing design codes, as shown in Fig. 27.

As shown, the fatigue strength at 2 million cycles of the established *S-N* curves with 95% survival probability is 93.2 MPa, which is the minimum value compared with that of the three existing design codes. The AASHTO [36] has the largest fatigue strength compared with the rest two design codes. The fatigue strengths of Eurocode 3 [38] and TB10091 [37] are close to each other. Besides, based on the S-N curves with 95% survival probability, the fatigue strength at 2 million cycles of the U-rib bolted joint (93.2 MPa) is 19.7 MPa larger than that of the U-rib butt-welded joint with root gap larger than or equal to 5 mm (73.5 MPa), this also indicates the former has a much better fatigue resistance than the latter.

4.2. Fatigue behavior evaluation of short-headed stud connectors

The short-headed stud connectors play a critical role to the integration of the OSD and UHPC layer and make the two components work together. Based on this beam test results listed in Table 5 and the results of literature [22], the shear fatigue *S-N* curves with 95% survival probability were established, as show in Fig. 28. Fig. 28 also shows the comparison of *S-N* curves from the beam test and from the push-out test. It should be noted that the push-out test conducted by Cao et al. [50] and Zhang et al. [51] was also for the short-headed stud connectors embedded in thin UHPC layer. As shown, the data points from the beam test lie above that from the push-out test, indicating that the short-headed stud connectors have a larger shear fatigue strength in the beam test than in the push-out test. This phenomenon was also found in relevant research [52] for stud connectors embedded in normal concrete slab. This result may be explained by the more pronounced shear stress distribution in the beam test than in the push-out test.

The obtained *S-N* curves with 95% survival probability from the beam test and the push-out test are compared with existing design codes, as shown in Fig. 29. The *S-N* curve from the beam test lies above all the design codes, indicating that the fatigue strength of the short-headed stud connectors in this specimen meet the design specification. Using the existing design codes to evaluate the fatigue behavior of the short-headed stud connectors in the OSD-UHPC composite decks will lead to a more conservative result. The *S-N* curve from the push-out test also lies above the design codes, and the fatigue strength at 2 million cycles of the push-out test is 8 MPa, 37 MPa and 43 MPa larger than that of Eurocode 4 [30], AASHTO [36] and TB10091 [37] respectively. The *S-N* curve from the push-out test ($\log N = 22.411\text{-}8\log\Delta\tau$) is recommended as the shear fatigue design curve of the short-headed stud connectors in the OSD-UHPC composite deck.

4.3. Fatigue behavior evaluation of UHPC member from different levels

4.3.1. Material level

The relevant UHPC standards [12,13] do not cover the tensile *S-N* curves because of the limited fatigue test data. The tensile *S-N* curves of UHPC and HPFRC (High performance fiber reinforced concrete) were gathered, as listed in Table 7 and plotted in Fig. 30. The fibers of UHPC

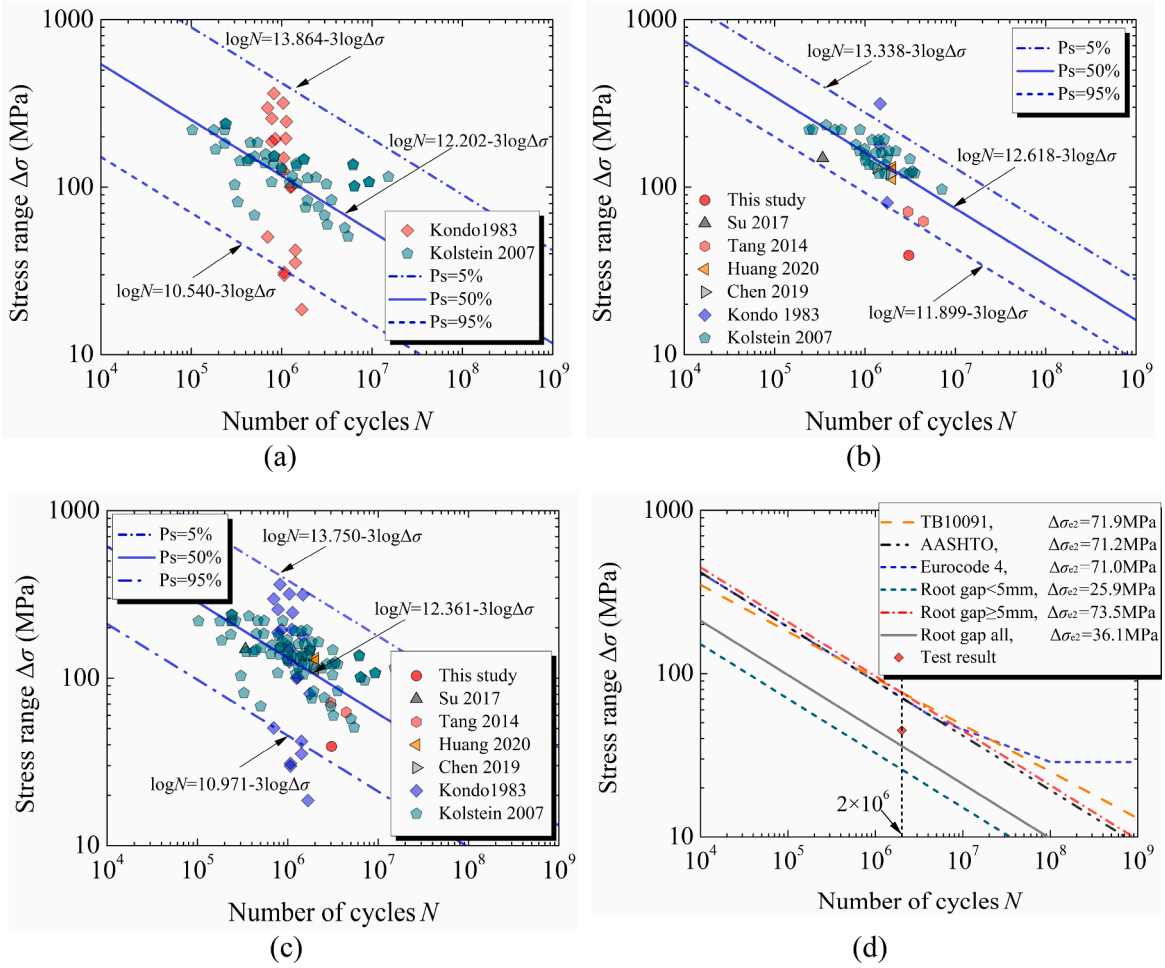

Fig. 26. *S-N* curves of the U-rib butt-welded joint : (a) root gap < 5 mm; (b) root gap ≥ 5 mm; (c) root gap all; (d) comparison with existing design codes.

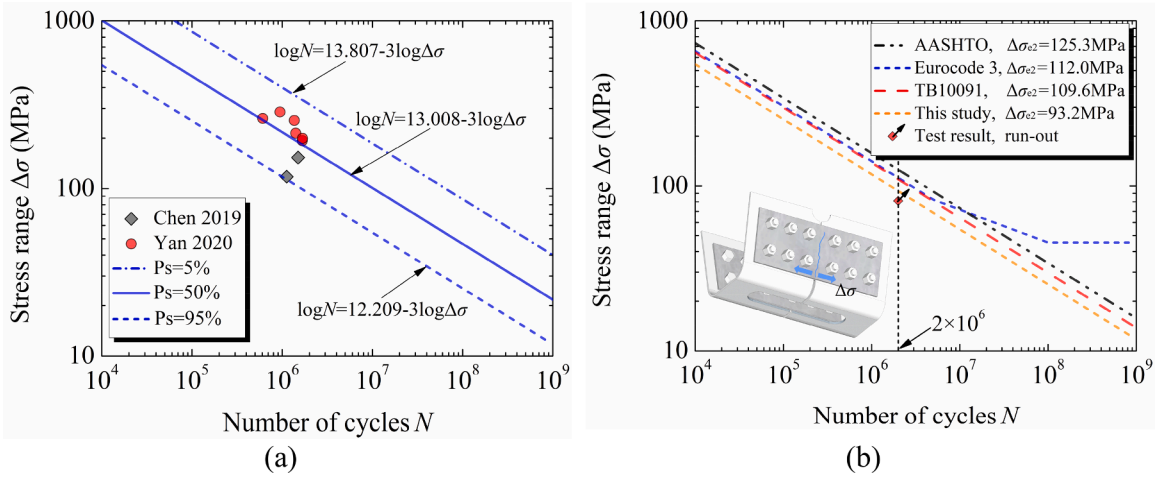

Fig. 27. *S-N* curves of U-rib bolted joint : (a) linear regression analysis; (b) comparison with existing design codes.

and HPFRC are short-thin steel fibers. The related testing methods are biaxial flexural test, four-point bending test (4PBT), three-point bending test (3PBT) and uniaxial direct tensile test (DTT). A unified fatigue failure criterion, i.e., fracture, which was reflected by unable to bear the maximum load of fatigue test, was adopted by these tests. In these fatigue tests, stress level S denotes the ratio of maximum stress for fatigue test to peak stress obtained from quasi-static test. As reported in literature [53,54], the dimensionless term S could effectively eliminate the difference from material properties, specimen sizes, test methods and loading conditions.

As plotted, the tensile fatigue stress levels at 2 million cycles, at 5 million cycles and at 10 million cycles range from 0.57 to 0.77, from 0.54 to 0.68, and from 0.52 to 0.67, respectively. The design fatigue stress levels at 2 million cycles, 5 million cycles and at 10 million cycles could be set as 0.55, 0.50 and 0.45 respectively considering the design safety.

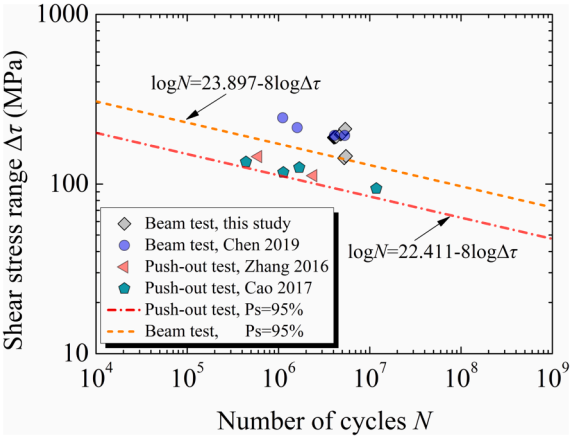

Fig. 28. Comparison of shear fatigue *S-N* curves from the beam test and the push-out test.

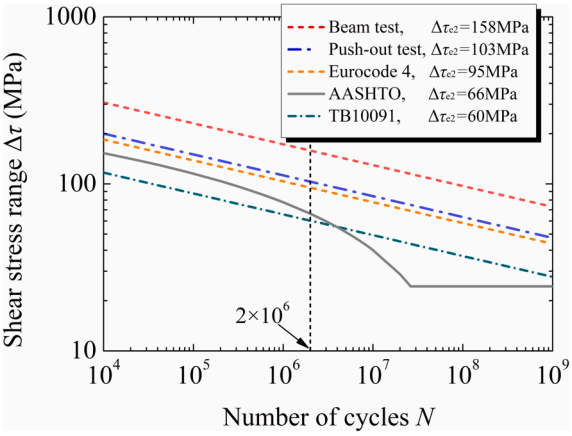

Fig. 29. Comparison of shear fatigue *S-N* curves with existing design codes.

4.3.2. Structural member level

The UHPC material is usually reinforced by rebar in real application, so the corresponding UHPC member could be defined as R-UHPC. The related fatigue failure tests of existing R-UHPC and R-SFRC (steel fiber reinforced concrete) are summarized, as listed in Table 8 and plotted in Fig. 31. The stress level S denotes the ratio of maximum load for fatigue test to peak load obtained from quasi-static test. The fatigue behavior of the R-UHPC and the R-SFRC member is determined by the material properties and the reinforcement ratio. The failure of the tensile fatigue test is usually defined by the fatigue fracture of the rebar while the crack width of concrete usually is larger than 0.2 mm. As shown in Fig. 31, the tensile fatigue stress levels at 2 million cycles, at 5 million cycles and at 10 million cycles range from 0.47 to 0.63, from 0.4 to 0.56, and from 0.34 to 0.55, respectively.

4.3.3. Structural system level

As discussed above, the tensile *S-N* curves of UHPC from the material level is established based on the fatigue fracture of the UHPC specimen. And the tensile *S-N* curves of R-UHPC from the structural member level is obtained based on the fatigue fracture of rebar. In real application, the fatigue fracture of the UHPC layer or of the rebar is not allowed to occur in the composite deck. Therefore, it is unreasonable to employ the *S-N* curves at the material and the structural member levels to evaluate the fatigue behavior of the UHPC layer in the composite deck. To ensure the stiffening effect of UHPC applied on the OSD, the cracking situation of UHPC layer is a concern of interest. According to the durability test conducted by Rafiee [31], the UHPC material behaves a sound material at critical crack width of 0.05 mm from the viewpoint of durability, for there are no corrosion occurring on steel fibers. The durability test also revealed that there is low amount of corrosion in specimens with crack width 0.10 mm, 0.15 mm, 0.2 mm and 0.3 mm. The French standard [13] for UHPC also specifies that the maximum crack width of reinforced UHPC members is 0.3 mm. In this view, the maximum critical crack width of UHPC in the OSD-UHPC composite deck should be set as 0.3 mm. Hence, it is necessary to establish the tensile *S-N* curves of the UHPC member based on the critical crack width of UHPC.

The relevant fatigue tests in which the crack width of UHPC layer exceeding 0.05 mm were limited. Therefore, the crack width of 0.05 mm could be chosen as the fatigue behavior evaluation index. The corresponding stress level $S_{w0.05}$ is then defined. The stress level $S_{w0.05}$ is the ratio of the maximum load of the fatigue load to the static load under which the crack width reaching 0.05 mm. The related fatigue test results were listed in Table 9. There is no relevant formula to transform the variable amplitude stress level to the constant amplitude stress level for the concrete materials. Considering the UHPC material behaves metalloid properties under uniaxial tension, the equivalent constant amplitude stress level of UHPC was obtained according to the formula used for fatigue details of steel structure [38],

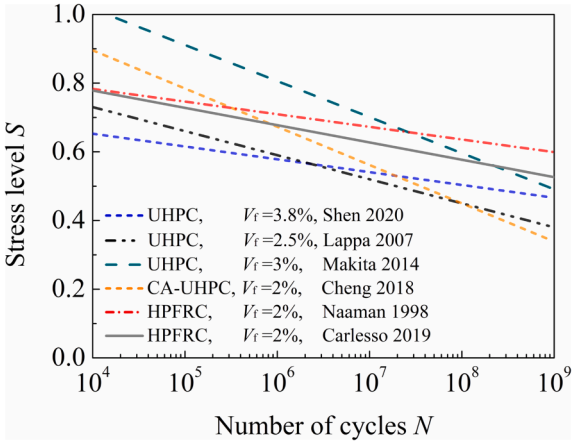

Fig. 30. Comparison of *S-N* curves for UHPC at the material level.

Table 7
S-N curves of UHPC and HPFRC under tensile fatigue loading.

Ref.	Material	V_f	Method	Failure criterion	σ_{min}	*S-N* curves
[54]	UHPC	3.8%	Biaxial flexural	fracture	$0.1\sigma_{max}$	$S = 0.8012–0.0372\log N$
[55]	UHPC	2.5%	4PBT		$0.2\sigma_{max}$	$S = 1.01–0.07\log N$
[56]	UHPC	3%	DTT		$0.1\sigma_{max}$	$\sigma_{max}/f_{ct,e} = 1.436–0.105\log N$
[57]	CA-UHPC	2%	4PBT		$0.1\sigma_{max}$	$S = 1.3406–0.1113\log N$
[58]	HPFRC	2%	4PBT		$0.1\sigma_p$	$S = 0.93–0.0368\log N$
[59]	HPFRC	2%	3PBT		$0.3\sigma_{max}$	$S = 0.9801–0.0504\log N$

Notes: V_f denotes fiber volume fraction. σ_p denotes peak tensile stress of the quasi-static test. σ_{max}, σ_{min} denote the maximum and the minimum tensile stress of the fatigue test. $f_{ct,e}$ denotes tensile elastic strength of UHPC under DTT.

Table 8
S-N curves of R-UHPC and R-SFRC members under tensile fatigue loading.

Ref.	Material	V_f	ρ	Method	Failure criterion	F_{min}	*S-N* curves
[56]	R-UHPC	3%	3.43%	DTT	Fracture of rebar	$0.1F_{max}$	$S = F_{max}/F_p = 1–0.065\log N$
[60]	R-SFRC	1%	1.40%	3PBT		$0.15F_p$	$S = 1.6065–0.1805\log N$
[61]	R-SFRC	1%	1.07%	4PBT		$0.1F_{max}$	$S = 1.8551–0.1943\log N$
[62]	R-SFRC	1%	0.94%	4PBT		$0.1F_p$	$S = 1.7827–0.2002\log N$

Notes: V_f denotes fiber volume fraction. ρ denotes reinforcement ratio. F_p denotes peak load of the quasi-static test. F_{max}, F_{min} denote the maximum and the minimum load of the fatigue test.

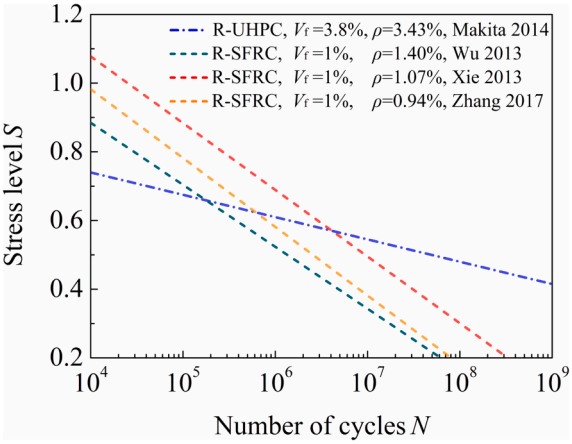

Fig. 31. Comparison of *S-N* curves for R-UHPC at the structural member level.

$$S_{w0.05} = \left[\frac{\sum N_i (S_{w0.05,i})^m}{N_f}\right]^{1/m} \quad (4)$$

where $S_{w0.05}$ is the equivalent constant stress level; N_f is the cyclic number at crack width of UHPC reaching 0.05 mm; $S_{w0.05,i}$ is the stress range at each loading phase; N_i is cyclic numbers corresponding to $S_{w0.05,i}$; m is taken as 3.

Based on the calculated equivalent constant stress level $S_{w0.05}$ and fatigue life N_f, the tensile *S-N* curve regarding critical UHPC crack width of 0.05 mm was obtained for the OSD-UHPC composite deck, as plotted in Fig. 32. The established *S-N* curve could be employed to evaluate the fatigue behavior of UHPC layer in the OSD-UHPC composite deck from the structural system level. This fatigue test could be considered as run-out because the maximum crack width of UHPC layer was only 0.04 mm.

4.4. Fatigue behavior evaluation of the composite deck system

The invention of the OSD-UHPC composite deck is to solve or alleviate the fatigue cracking problems of welded joints of the OSD. The composite effect is achieved by the connecting role of the short-headed stud connectors welded on the steel deck plate. Therefore, the fatigue performance of composite deck system depends on the fatigue resistance of the short-headed studs at the interface. As compared above, the shear fatigue strength of the short-headed stud connectors from the beam test is 55 MPa larger than that from the push-out test. Considering the design safety, the global fatigue performance of the composite deck could be evaluated by the *S-N* curve with 95% survival probability ($\log N = 22.411\text{-}8\log\Delta\tau$) from the push-out test for the short-headed stud connectors.

In addition, there shouldn't be any new fatigue-prone details occurring in the composite deck compared with the traditional OSD, for example the fatigue tearing off of the steel deck plate around the welded short-headed studs. The tearing off of the steel deck plate is caused by the relatively large ratio of the stud diameter to steel plate thickness according to Wang et al.[65].Therefore, more fatigue tests should be conducted to reveal the underlying mechanism and to prevent the occurrence of this failure mode.

5. Conclusions

Based on the above investigations, the main conclusions are:

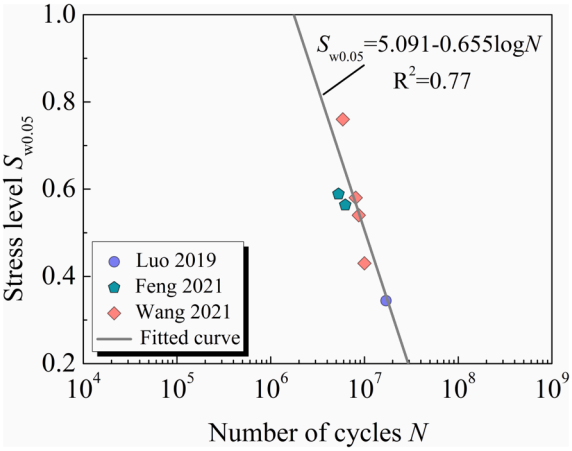

Fig. 32. *S-N* curves for UHPC layer at the structural system level.

Table 9
Fatigue test results of UHPC layer of OSD-UHPC composite decks in existing literatures.

Ref.	Specimen Number	Loading style	Loading phase	$S_{w0.05,\,i}$	N_i ($\times 10^4$)	$S_{w0.05}$	N_f ($\times 10^4$)
[63]	—	VA	I	0.24	1000	0.34	1697
			II	0.43	697		
[18]	Spacing-80 mm	VA	I	0.36	270	0.59	529
			II	0.55	100		
			III	0.73	100		
			IV	0.87	59		
[64]	F-S1	CA	I	0.43	1000	0.43	1000
	F-S2		I	0.54	870	0.54	870
	F-S3		I	0.76	588	0.76	588
	F-S4		I	0.58	808	0.58	808

Notes: VA denotes variable amplitude cyclic loading, CA denotes constant amplitude cyclic loading.

(1) Under the cyclic loading, the crack on U-rib initiating from weld toe at the bottom of the rib-to-cross beam welded joint firstly occurred. Then cracks on the U-rib butt-welded joint came to initiate and propagate along the weld length, followed by interface debonding between the steel deck plate and the UHPC layer. The UHPC layer exhibited short-thin cracks with maximum crack width reaching 0.04 mm. The fatigue damage occurred at the OSD, the interface and the UHPC layer did not significantly reduce the global stiffness of the composite deck system.
(2) The U-rib bolted joint exhibits better fatigue resistance than the U-rib butt-welded joint with backing strip under the same loading condition. Based on the established *S-N* curves with 95% survival probability, the fatigue strength at 2 million cycles of the U-rib bolted joint (93.2 MPa) is 19.7 MPa larger than that of the U-rib butt-welded joint (73.5 MPa) with weld root gap larger than or equal to 5 mm.
(3) The fatigue failure modes of the short-headed stud connectors could be classified into 5 types exhibiting the fracture of stud shank and tearing off of the steel deck plate. The established *S-N* curves with 95% survival probability ($\log N = 22.411\text{-}8\log\Delta\tau$) from the push-out test could be used to assess the global fatigue performance of the OSD-UHPC composite deck.
(4) The tensile *S-N* curves for UHPC at the material and the structural member levels are unsuitable to make assessment of fatigue resistance of UHPC layer in the composite deck. Considering the durability-based critical crack width of UHPC, the established tensile *S-N* curve ($S_{w0.05} = 5.091\text{–}0.655\log N$) regarding critical UHPC crack width of 0.05 mm could be used to assess the anti-fatigue cracking ability of UHPC layer in the composite deck system.

CRediT authorship contribution statement

Zhanchong Shi: Methodology, Investigation, Formal analysis, Writing – original draft, Writing – review & editing. **Qingtian Su:** Supervision, Investigation, Writing – review & editing. **Florentia Kavoura:** Supervision, Writing – review & editing. **Milan Veljkovic:** Supervision, Writing – review & editing.

Declaration of Competing Interest

The authors declare that they have no known competing financial interests or personal relationships that could have appeared to influence the work reported in this paper.

Data availability

Data will be made available on request.

Acknowledgements

This research was supported by the National Natural Science Foundation of China (NO. 51978501), the Jiangxi Province Major Research and Development Program (No. 20165ABC28001), the Fujian Transportation Science and Technology Project (No.202126). These programs are gratefully acknowledged.

References

[1] Kolstein MH. Fatigue Classification of Welded Joints in Orthotropic Steel Bridge Decks. Delft, the Netherlands: Delft University of Technology; 2007. Doctoral Thesis,.
[2] Walter R, Olesen JF, Stang H, Vejrum T. Analysis of an Orthotropic Deck Stiffened with a Cement-Based Overlay. J Bridg Eng 2007;12:350–63. https://doi.org/10.1061/(asce)1084-0702(2007)12:3(350).
[3] Shao X, Yi D, Huang Z, Zhao H, Chen B, Liu M. Basic Performance of the Composite Deck System Composed of Orthotropic Steel Deck and Ultrathin RPC Layer. J Bridg Eng 2013;18:417–28. https://doi.org/10.1061/(asce)be.1943-5592.0000348.
[4] Cui C, Bu Y, Bao Y, Zhang Q, Ye Z. Strain Energy-Based Fatigue Life Evaluation of Deck-to-Rib Welded Joints in OSD Considering Combined Effects of Stochastic Traffic Load and Welded Residual Stress. J Bridg Eng 2018;23:04017127. https://doi.org/10.1061/(asce)be.1943-5592.0001181.
[5] Cheng B, Ye X, Cao X, Mbako DD, Cao Y. Experimental study on fatigue failure of rib-to-deck welded connections in orthotropic steel bridge decks. Int J Fatigue 2017;103:157–67. https://doi.org/10.1016/j.ijfatigue.2017.05.021.
[6] Zhao Q, Guo Z, Shen X, Briseghella B. Test study on residual stress distribution of hybrid steel u-rib stiffened plates. J Constr Steel Res 2016;121:261–7. https://doi.org/10.1016/j.jcsr.2016.01.024.
[7] Buitelaar P, Braam R, Kaptijn N. Reinforced high performance concrete overlay system for rehabilitation and strengthening of orthotropic steel bridge decks. USA: Orthotropic Bridg Conf Sacramento; 2004. p. 384–401.
[8] Ma CH, Deng P, Matsumoto T. Fatigue analysis of a UHPFRC-OSD composite structure considering crack bridging and interfacial bond stiffness degradations. Eng Struct 2021;249:113330. https://doi.org/10.1016/j.engstruct.2021.113330.
[9] Murakoshi J, Yanadori N, Ishii H. Research on steel fiber reinforced concrete pavement for orthotropic steel deck as a countermeasure for fatigue. Proc., 23th U. S.-Japan Bridg. Eng. Work., Ibaraki-Ken: Public Works Research Institute of Japan; 2007.
[10] Dieng L, Marchand P, Gomes F, Tessier C, Toutlemonde F. Use of UHPFRC overlay to reduce stresses in orthotropic steel decks. J Constr Steel Res 2013;89:30–41. https://doi.org/10.1016/j.jcsr.2013.06.006.
[11] Haber ZB, la Varga ID, Graybeal BA, Nakashoji B, El-Helou R. Properties and Behavior of UHPC-Class Materials. Fhwa-Hrt-18-036 2018:153.
[12] MCS-EPFL. Ultra-High Performance Fibre Reinforced Cement-based composites (UHPFRC) Construction material , dimensioning und application. Lausanne, Switzerland; 2016.
[13] Association Francaise de Normalisation. Concrete-ultra-high performance fibre-reinforced concrete-specifications, performance, production and conformity. NF P; 2016.
[14] Cao J, Shao X, Zhang Z, Zhao H. Retrofit of an orthotropic steel deck with compact reinforced reactive powder concrete. Struct Infrastruct Eng 2016;12:411–29. https://doi.org/10.1080/15732479.2015.1019894.
[15] Shao X, Cao J. Fatigue Assessment of Steel-UHPC Lightweight Composite Deck Based on Multiscale FE Analysis: Case Study. J Bridg Eng 2018;23:05017015. https://doi.org/10.1061/(asce)be.1943-5592.0001146.
[16] Wang Y, Shao X, Chen J, Cao J, Deng S. UHPC-based strengthening technique for orthotropic steel decks with significant fatigue cracking issues. J Constr Steel Res 2021;176:106393. https://doi.org/10.1016/j.jcsr.2020.106393.
[17] Zhu Z, Xiang Z, Zhou YE. Fatigue behavior of orthotropic steel bridge stiffened with ultra-high performance concrete layer. J Constr Steel Res 2019;157:132–42. https://doi.org/10.1016/j.jcsr.2019.02.025.
[18] Feng Z, Li C, He J, Ke L, Lei Z, Vasdravellis G. Static and fatigue test on lightweight UHPC-OSD composite bridge deck system subjected to hogging moment. Eng Struct 2021:241. https://doi.org/10.1016/j.engstruct.2021.112459.
[19] Unterweger H, Novak F. 21.02: Strengthening of orthotropic steel decks using UHPC: UHPC-concrete instead of asphalt layer for additional at least 50 years in service. Ce/Papers 2017;1:4502–11. https://doi.org/10.1002/cepa.510.
[20] Yuan Y, Wu C, Jiang X. Experimental study on the fatigue behavior of the orthotropic steel deck rehabilitated by UHPC overlay. J Constr Steel Res 2019;157:1–9. https://doi.org/10.1016/j.jcsr.2019.02.010.
[21] Liu Y, Zhang Q, Meng W, Bao Y, Bu Y. Transverse fatigue behaviour of steel-UHPC composite deck with large-size U-ribs. Eng Struct 2019;180:388–99. https://doi.org/10.1016/j.engstruct.2018.11.057.
[22] Chen S, Huang Y, Gu P, Wang JY. Experimental study on fatigue performance of UHPC-orthotropic steel composite deck. Thin-Walled Struct 2019;142:1–18. https://doi.org/10.1016/j.tws.2019.05.001.
[23] Ministry of Transport of the People's Republic of China, JTG D64-2015. Specifications for Design of Highway Steel Bridge. China Communications Press, Beijing; 2015.
[24] General Administration of Quality Supervision, Inspection and Quarantine of the People's Republic of China, GB/T 10433-2002. Cheese head studs for arc stud welding; 2002.
[25] Ministry of Transport of the People's Republic of China. JTG 3362-2018. Specifications for Design of Highway Reinforced Concrete and Prestressed Concrete Bridges and Culverts. China Communications Press, Beijing; 2018.
[26] General Administration of Quality Supervision, Inspection and Quarantine of the People's Republic of China,. GB/T 228-2202. Metallic materials-Tensile testing at ambient temperature; 2002.
[27] China Association for Engineering Construction Standardization. CECS13:2009. Beijing: Standard test methods for fiber reinforced concrete. China Plan. Press; 2009.
[28] Shi Z, Su Q, Kavoura F, Veljkovic M. Behavior of short-headed stud connectors in orthotropic steel-UHPC composite bridge deck under fatigue loading. Int J Fatigue 2022;160:106845. https://doi.org/10.1016/j.ijfatigue.2022.106845.
[29] Miner MA. Cumulative Damage in Fatigue. J Appl Mech 1945;12:A159–64. https://doi.org/10.1115/1.4009458.
[30] European Committee for Standardization, Eurocode 4: Design of composite steel and concrete structures-Part 2: Composite bridges. Belgium; 2005.
[31] Rafiee A. Computer Modeling and Investigation on the Steel Corrosion in Cracked Ultra High Performance Concrete. Kassel, Germany: Kassel University; 2003. Doctoral Thesis,.
[32] Zhang Q, Liu Y, Bao Y, Jia D, Bu Y, Li Q. Fatigue performance of orthotropic steel-concrete composite deck with large-size longitudinal U-shaped ribs. Eng Struct 2017;150:864–74. https://doi.org/10.1016/j.engstruct.2017.07.094.

[33] Liu Y. Fatigue failure mechanism of steel-high performance concrete composite bridge deck with large-size u-ribs. Chengdu, China: Southwest Jiaotong University; 2019. Doctoral Thesis,[in Chinese].
[34] Liu Y, Zhang Q, Bao Y, Bu Y. Fatigue behavior of orthotropic composite deck integrating steel and engineered cementitious composite. Eng Struct 2020;220:111017. https://doi.org/10.1016/j.engstruct.2020.111017.
[35] Ding N, Shao X. Study on fatigue performance of light-weighted composite bridge deck. China Civ Eng J 2015;48:74–81 [in Chinese]. https://doi.org/10.15951/j.tmgcxb.2015.01.009.
[36] American Association of State Highway and Transportation Officials. AASHTO LRFD bridge design specifications. Washington DC, USA; 2007.
[37] National Railway Administration of the People's Republic of China. TB 10091-2017. Code for Design on Steel Structure of Railway Bridge. China Railway Publishing House, Beijing; 2017.
[38] European Committee for Standardization. Eurocode 3: Design of steel structures-Part 1-9:Fatigue. Belgium; 2006.
[39] Wang C, Fu B, Zhang Q, Feng Y. Fatigue test on full-scale orthotropic steel bridge deck. China J Highw Transp 2013;26:69–76 [in Chinese]. https://doi.org/10.19721/j.cnki.1001-7372.2013.02.011.
[40] Zhang QH, Cui C, Bu YZ, Liu YM, Ye HW. Fatigue tests and fatigue assessment approaches for rib-to-diaphragm in steel orthotropic decks. J Constr Steel Res 2015;114:110–8. https://doi.org/10.1016/j.jcsr.2015.07.014.
[41] Huang Y, Zhang Q, Bao Y, Bu Y. Fatigue assessment of longitudinal rib-to-crossbeam welded joints in orthotropic steel bridge decks. J Constr Steel Res 2019;159:53–66. https://doi.org/10.1016/j.jcsr.2019.04.018.
[42] Zhang Q, Li J, Yuan D, Zhu J, Cui C. Fatigue model tests of orthotropic steel bridge deck of Shenzhen-Zhongshan Link. China Civ Eng J 2020;53:102–15 [in Chinese]. https://doi.org/10.15951/j.tmgcxb.2020.11.011.
[43] Hobbacher AF. Erratum to: Recommendations for Fatigue Design of Welded Joints and Components. 2019. https://doi.org/10.1007/978-3-319-23757-2_8.
[44] Kondo A, Yamada K, Hisao Aoki YK. Fatigue strength of field-welded trough rib joints of orthotropic steel decks. Proc. Japan Soc. Civ. Eng. 1983:49–57.
[45] Su Q, He X, Zeng M. Experiment research on fatigue faiure and repair method for butt weld in U-shaped rib of composite bridge deck. J Tongji Univ Sci 2017;45:167–72 [in Chinese].
[46] Tang L, Huang L, Liu G, Wang C, Fu B. Fatigue experimental study of a full-scale steel orthotropic deck model. China Civ Eng J 2014;47:112–22 [in Chinese]. https://doi.org/10.15951/j.tmgcxb.2014.03.006.
[47] Chen S, Huang Y, Zhou C, Gu P. Experimental and numerical study on fatigue performance of U-rib connections. J Constr Steel Res 2019;163:105796. https://doi.org/10.1016/j.jcsr.2019.105796.
[48] Huang Z, Lei J, Guo S, Tu J. Fatigue performance of U-rib butt welds in orthotropic steel decks. Eng Struct 2020;211:110485. https://doi.org/10.1016/j.engstruct.2020.110485.
[49] Yan F. The research of the fatigue property of site-butt of orthotropic steel bridge deck. Beijing, China: North China University of Technology; 2018. Master's Thesis, [in Chinese].
[50] Cao J, Shao X, Deng L, Gan Y. Static and Fatigue Behavior of Short-Headed Studs Embedded in a Thin Ultrahigh-Performance Concrete Layer. J Bridg Eng 2017;22:04017005. https://doi.org/10.1061/(asce)be.1943-5592.0001031.
[51] Zhang S. Basic performance of a lightweight composite bridge deck with open ribs. Changsha, China: Hunan University; 2016. Master's Thesis,[in Chinese].
[52] Roberts TM, Dogan O. Fatigue of Welded Stud Shear Connectors in Steel-Concrete-Steel Sandwich Beams. J Constr Steel Res 1998;45:301–20. https://doi.org/10.1016/S0143-974X(97)00070-9.
[53] Lee MK, Barr BIG. An overview of the fatigue behaviour of plain and fibre reinforced concrete. Cem Concr Compos 2004;26:299–305. https://doi.org/10.1016/S0958-9465(02)00139-7.
[54] Shen X, Brühwiler E. Biaxial flexural fatigue behavior of strain-hardening UHPFRC thin slab elements. Int J Fatigue 2020;138:105727. https://doi.org/10.1016/j.ijfatigue.2020.105727.
[55] Lappa ES. High Strength Fibre Reinforced Concrete: Static and fatigue behaviour in bending. Delft, the Netherlands: Delft University of Technology; 2007. Doctoral Thesis,.
[56] Makita T, Brühwiler E. Tensile fatigue behaviour of ultra-high performance fibre reinforced concrete (UHPFRC). Mater Struct Constr 2014;47:475–91. https://doi.org/10.1617/s11527-013-0073-x.
[57] Cheng J. Study on flexural fatigue performance of ultra high performance concrete with coarse aggregate. Nanjing, China: Dongnan University; 2018. Master's Thesis, (in Chinese.
[58] Naaman AE, Hammoud H. Fatigue characteristics of high performance fiber-reinforced concrete. Cem Concr Compos 1998;20:353–63. https://doi.org/10.1016/S0958-9465(98)00004-3.
[59] Carlesso DM, de la Fuente A, Cavalaro SHP. Fatigue of cracked high performance fiber reinforced concrete subjected to bending. Constr Build Mater 2019;220:444–55. https://doi.org/10.1016/j.conbuildmat.2019.06.038.
[60] Wu J. Experimental studies and numerical analysis of fatigue properties of steel fiber reinforced concrete beam. Zhengzhou, China: Zhengzhou University; 2013. Master's Thesis,[in Chinese].
[61] Xie Y. Experimental study on the properties of steel fiber reinforced concrete beams under flexural fatigue loading. Hohhot, China: Inner Mongolia University of Technology; 2013. Master's Thesis,[in Chinese].
[62] Zhang S. Steel fiber reinforced high-strength concrete beam fatigue test research. Zhengzhou, China: Zhengzhou University; 2017. Master's Thesis,[in Chinese].
[63] Luo J. Research on mechanical performance and crack width calculation theory of steel-UHPC lightweight composite deck structures. Changsha, China: Hunan University; 2019. Doctoral Thesis,[in Chinese].
[64] Wang Y, Shao X, Shen X, Cao J. Experiment on static and fatigue performances of steel strip-UHPC composite deck. China J Highw Transp 2021;34:261–72 [in Chinese].
[65] Yu-Hang W, Jian-Guo N, Jian-Jun L. Study on fatigue property of steel-concrete composite beams and studs. J Constr Steel Res 2014;94:1–10. https://doi.org/10.1016/j.jcsr.2013.11.004.